HHS Public Access

Author manuscript

Immunity. Author manuscript; available in PMC 2020 April 30.

Published in final edited form as:

Immunity. 2019 January 15; 50(1): 121–136.e5. doi:10.1016/j.immuni.2018.11.003.

Age-related loss of innate immune antimicrobial function of dermal fat is mediated by transforming growth factor beta

Ling-juan Zhang[1,2,*], **Stella Xiang Chen**[2], **Christian F. Guerrero-Juarez**[3,4], **Fengwu Li**[2], **Yun Tong**[2], **Yuqiong Liang**[6], **Marc Liggins**[2], **Xu Chen**[5], **Hao Chen**[5], **Min Li**[5], **Tissa Hata**[2], **Ye Zheng**[6], **Maksim V. Plikus**[3,4], **Richard L. Gallo**[2,7,*]

[1]School of Pharmaceutical Sciences, Xiamen University, Xiamen, China.

[2]Department of Dermatology, University of California, San Diego, La Jolla, CA 92093, USA.

[3]Department of Developmental and Cell Biology, Sue and Bill Gross Stem Cell Research Center, University of California, Irvine, Irvine, CA 92697, USA.

[4]Center for Complex Biological Systems, University of California, Irvine, Irvine, CA 92697, USA.

[5]Institute of Dermatology, Jiangsu Key Laboratory of Molecular Biology for Skin Diseases and STIs, Chinese Academy of Medical Science and Peking Union Medical College, Nanjing 210042, China

[6]Nomis Foundation Laboratories for Immunobiology and Microbial Pathogenesis, The Salk Institute for Biological Studies, La Jolla, California 92037, USA.

[7]Lead contact

Summary

Dermal fibroblasts (dFB) resist infection by locally differentiating into adipocytes and producing the antimicrobial peptide cathelicidin in response to *S. aureus*. Here we showed that neonatal skin was enriched with adipogenic dFB and immature dermal fat that highly expressed cathelicidin.. The pool of adipogenic and antimicrobial dFB declined after birth, leading to an age-dependent loss of dermal fat and a decrease of adipogenesis and *Camp* production in response to infection. Transforming growth factor beta (TGFβ) was identified as a key upstream regulator of this process that acted on uncommitted embryonic and adult dFB and inhibited their adipogenic and

*Correspondence: lingjuan.zhang@xmu.edu or l6zhang@ucsd.edu (L.J.Z.); or rgallo@ucsd.edu (R.L.G).

Author Contributions

L.Z. performed experiments, interpreted data, co-directed the study and wrote the manuscript; S.C., F.L., and M.L. provided experimental assistance for primary culture and in vitro assays and in vivo mouse skin infection studies. C.F.G-J performed SMART-seq2, transcript alignment, quantification, filtering and analyses and revised the manuscript. L.Y. and T.H. provided human healthy adult human biopsies from the UCSD dermatology clinics and C.Y., H.C. and M.L. provided healthy human skin biopsies from Dermatology clinics in China. Y.L. and Y.Z. performed flow cytometry analyses of dermal myeloid immune cells. M.V.P. provided reagents and expertise related to RNA-seq study and revised the manuscript. R.L.G. interpreted data, directed the studies and wrote the manuscript.

Disclosures

R.L.G. serves on the scientific advisory board and is a consultant for Sente and MatriSys Bioscience and has equity interest.

antimicrobial function. Furthermore, inhibition of the TGFβ receptor restored the adipogenic and antimicrobial function of dFB in culture and increased resistance of adult mice to *S. aureus* infection. These results provide insight into changes in the skin innate immune system that occur between the perinatal and adult periods of life.

eTOC blurb

Dermal immature adipocytes fight against *Staphylococcus aureus* infection by secreting antimicrobial peptides during adipogenesis. Zhang et al. demonstrate that activation of the TGFβ pathway suppresses the adipogenic potential of dermal fibroblasts and therefore leads to an age-dependent loss of antimicrobial protection from dermal fat.

Graphical Abstract

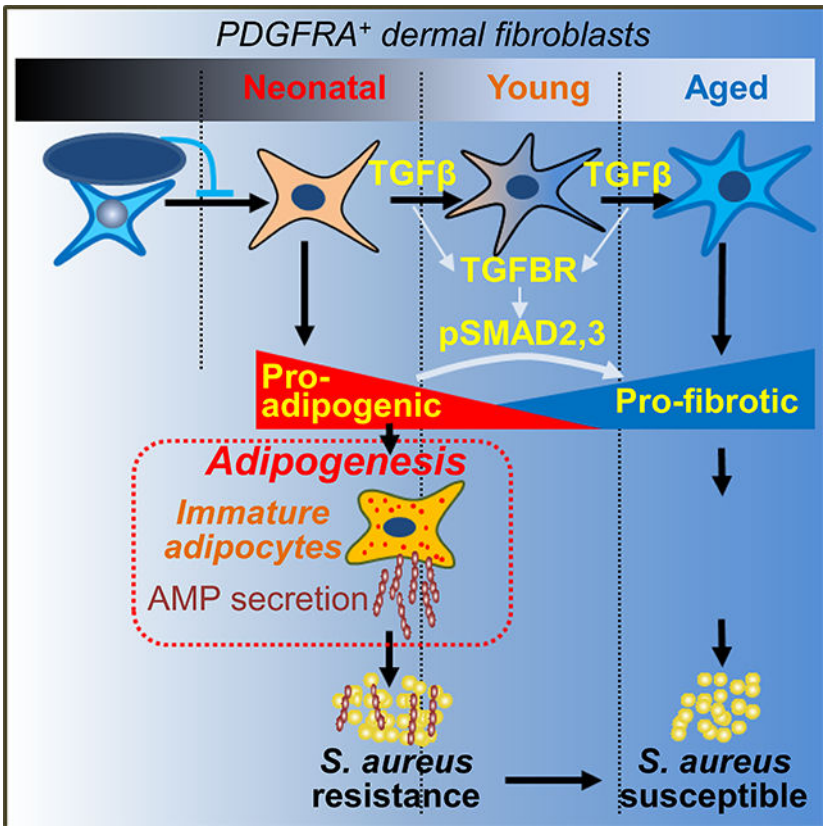

Keywords

Innate immunity; dermal white adipose tissue; dermal fibroblasts; adipocyte progenitors; adipocytes; *Staphylococcus aureus*; infection; cathelicidin; antimicrobial peptides; Transforming growth factor beta

Introduction

Staphylococcus aureus (*S. aureus*) is responsible for the majority of skin and soft tissue infections in humans, and MRSA (methicillin-resistant *S. aureus*) infections during the past two decades are responsible for more deaths in the United States than any other pathogen (Klein et al., 2007; Miller and Cho, 2011). Infections with *S. aureus* are difficult to treat because of evolved resistance to common antibiotics; therefore, a better understanding of skin host defense mechanisms against *S. aureus* is acutely needed for developing strategies to combat this important public health problem.

Skin provides a physical and immunological barrier protecting internal tissues from external insults. Dermal white adipose tissue (dWAT) is the deepest barrier of the skin and an understudied fat depot compared to inguinal fat (iWAT) and epididymal fat (eWAT) (Zwick et al., 2018). Until recently, dWAT has been thought to function merely as an energy reservoir and a thermo-insulating layer. Recent studies, however, have revealed that dWAT also plays active roles in various physiological and pathological processes such as hair follicle regeneration (Festa et al., 2011), wound healing (Plikus et al., 2017; Schmidt and Horsley, 2013), thermogenesis (Kasza et al., 2014), skin fibrosis (Marangoni et al., 2015), and protection against skin infection (Zhang et al., 2015). DWAT is produced by a subpopulation of dermal fibroblasts (dFB). dFB are a major cell type in the skin that have considerable functional diversity (Philippeos et al., 2018; Tabib et al., 2018). The reticular dermis contains dFB with adipocyte progenitor properties, and they can commit to preadipocytes (pAd) and differentiate into adipocytes (AD) upon stimulation (Driskell et al., 2013; Festa et al., 2011; Schmidt and Horsley, 2013; Zhang et al., 2015).

S. aureus skin infection triggers the rapid and localized differentiation of pAd to AD, and we refer to this process as reactive adipogenesis. Reactive adipogenesis is characterized by the proliferation of adipocyte progenitor cells expressing Preadipocyte factor 1 positive ($PREF1^{+}$) and is followed by their differentiation to immature AD (Zhang et al., 2015). During this process, the antimicrobial peptide (AMP) cathelicidin (*Camp*) is abundantly expressed during the immature AD stage of differentiation. This expression of *Camp* is necessary to limit bacterial spread since inhibition of this adipogenic-antimicrobial function of immature AD leads to increased susceptibility to *S. aureus* infection (Zhang et al., 2015).

In this study, we sought to better understand the regulation of reactive adipogenesis in skin innate immunity. To explore this question, we investigated changes in adipogenic function of dFB during embryonic and adult development in mouse and human skin. A decrease in the capacity of dFB to differentiate into adipocytes and express cathelicidin was observed to occur after birth and during the adult period of life. Furthermore, Transforming growth factor beta (TGFβ) was identified to induce the loss of adipogenic potential and antimicrobial function of dFB. These results uncover a previously unknown mechanism that impairs innate immune defense of the skin.

Results

Dermal PDGFRA^{+}THY1^{hi} adipocyte progenitors and their antimicrobial response are lost with advancing age

To establish the relative contribution from cells of the adipocyte lineage to express cathelicidin, mice were generated to permit conditional deletion of *Camp* by inserting *LoxP* sites flanking exons 2~4 (Fig. 1A). These *Camp$^{flox/flox}$* mice were crossed with *Pdgfra-cre* or *Adipoq-cre* mice to delete *Camp* in dFB that express *Pdgfra* (*Camp$^{f/f}$Pdgfra-cre*) or cells in the later pAD stage that express *Adipoq* (*Camp$^{f/f}$Adipoq-cre*). Flow cytometry and RTqPCR validated that *Pdgfra* or *cre* expression was highly enriched on THY1^{+}CD45^{-} dermal fibroblasts (dFB) but not in THY1^{-}CD45^{+} myeloid immune cells or spleen tissue (Fig. S1A–B). Upon *S. aureus* infection, *Camp* expression was significantly suppressed in the *Camp$^{f/f}$Pdgfra-cre* or *Camp$^{f/f}$Adipoq-cre* skin, but not in the spleen or blood cells (Fig. 1B and S1C–E). *Camp$^{f/f}$Pdgfra-cre* and *Camp$^{f/f}$Adipoq-cre* mice became significantly more susceptible to *S. aureus* infection compared to WT littermate controls (Fig. 1C and Fig. S1F–H). These results reinforced the conclusion that cathelicidin derived from cells of the adipocyte lineage plays a role in defense against *S. aureus* infection.

In general, innate immune defense is maximal in late fetal and early postnatal life and declines with aging (Futata et al., 2012; Georgountzou and Papadopoulos, 2017; Shaw et al., 2013). An age-dependent decrease of the ability of skin to clear bacteria was seen by increased bacterial CFU in the infection edge area with advancing age (Fig. 1D and S1I). To understand the contribution of adipogenesis to this loss of innate immune defense, we next examined the expression of cathelicidin in the cells of the adipocyte lineage during aging. A progressive loss of the capacity of *S. aureus* to trigger reactive adipogenesis was observed with advancing age, as measured by lesser staining of cathelicidin (Fig. 1E) and lower expression of *Pref1* and *Camp* mRNA (Fig. S1J and Fig. 1F) in dWAT at sites of infection. Loss of dermal reactive adipogenesis in response to *S. aureus* correlated with an age-dependent increase in the mRNA expression of *Spp1*, a pro-fibrotic marker (Fig. 1F).

Next, we established a flow cytometry method to define cell populations within dFB that are activated upon *S. aureus* infection. Adipogenic dFB were gated as CD31^{-};CD45^{-};PDGFRA^{+};THY1^{hi} cells (Chia et al., 2016; Rivera-Gonzalez et al., 2016). *S. aureus* infection triggered an increase in surface expression of PDGFRA and Sca1 in THY1^{hi};PDGFRA^{+} cells but not in THY1^{lo};PDGFRA^{+} cells (Fig. 1G–1H and Fig. S1K). This suggested that reactive adipogenesis was restricted to THY1^{hi} dFB. To determine whether age-related loss of reactive adipogenesis was associated with the loss of THY1^{hi} dFB, THY1 expression was analyzed in PDGFRA^{+} dFB in the late embryo and in mice up to 2 years of age. Fibroblasts from eWAT were also analyzed because eWAT has been previously reported to have age-associated dysfunction in adipogenesis and increased production of pro-inflammatory cytokines and fibrotic features (Kirkland et al., 1993; Sun et al., 2013). Flow cytometry analyses revealed that PDGFRA^{+} fibroblasts in eWAT progressively lost THY1 expression with advancing age (from 3 weeks, 2 months, 1 year to 2 years), and by 1~2 years of age PDGFRA^{+} fibroblasts in eWAT were mostly THY1^{lo} (Fig. 1I–K). In the skin, E14 embryonic PDGFRA^{+} dFB were mostly THY1^{lo} (>97%), and became mostly THY1^{hi}

(>90%) by postnatal day 1 (P1). Similar to eWAT, THY1 expression became then progressively lost in dermal PDGFRA^{+} fibroblasts during postnatal development and aging (Fig. 1I–K). Thus, age-related loss of THY1 expression is a common feature of PDGFRA^{+} fibroblasts in both eWAT and skin.

Next, age-related changes in PDGFRA^{+} dFB were evaluated in parallel with changes in myeloid or lymphoid-derived immune cells, including CD11B^{+}F4/80^{+} macrophage, CD11B^{+}Ly6G^{hi} neutrophils, CD11C^{+}F4/80^{-} dendritic cells (DC), CD45^{+} T cell receptor(TCR)$\gamma\delta^{+}$ T cells and CD45^{+}TCR$\alpha\beta^{+}$ T cells (Fig. 1L and S1M–N). PDGFRA^{+}THY1^{hi} dFB represented the major resident innate cell type (~75% of total dermal cells) in neonatal (P1) skin. During postnatal development (3 weeks~2 months), the decline in THY1^{hi} dFB was accompanied by an increase in myeloid-derive immune cell populations. Upon aging (1~2 years), the THY1^{hi} dFB population continued to decline, as did macrophages and DCs, whereas CD45^{+}TCR$\alpha\beta^{+}$ cells increased both in the skin and in eWAT (Fig. 1L and S1M–N)..

Next we characterized if age-related changes of adipogenic dFB correlated with changes in dermal fibrogenesis and adipogenesis. As shown in Fig. 2A, while dWAT and the fibrogenic features (collagen staining and dermal hydroproline content) of dermis were not developed in E14 skin, neonatal skin featured large dWAT with immature adipocytes and numerous small lipid droplets (Fig. 2A–2B and S2A). Dermal adipocytes matured (indicated by large lipid droplets) by 3 weeks of age and were then gradually lost during adulthood and aging (2 months through 2 years) (Fig. 2A). Loss of immature dermal fat with advancing age was also supported by early peak at P1 in the mRNA expression of *Pref1* and *Camp,* genes associated with early adipogenesis, followed by their progressive decline from postnatal development through aging (Fig. 2C–D). Immunostaining for cathelicidin confirmed that it was abundantly expressed by P1 immature dermal AD whereas its expression was decreased in mature 3 week AD and became undetectable in the 1 year aged AD (Fig. S2B). Deletion of *Camp* in Pdgfra^{+} dFB (*Camp*$^{f/f}$*Pdgfra-cre*) or Adipoq^{+} AD (*Camp*$^{f/f}$*Adipoq-cre*) led to >95% and ~75% reduction in *Camp* mRNA expression in neonatal skin, respectively (Fig. 2E), confirming that differentiating immature AD are the major cellular source of cathelicidin in neonatal skin. The expression of mature adipocyte markers, including *Adipoq* and *Fabp4*, peaked at 3 weeks ~ 2 months, then decreased progressively from 2 months~2 years (Fig. 2C and S2C), supporting our histological observation that mature AD were lost with age. Age-dependent loss of immature dermal fat coincided with an age-dependent gain in dermal fibrotic features, especially in the dWAT layer, as shown by collagen staining, hydroxyproline measurement and *Col1a1* mRNA expression (Fig. 2A–2C and S2D). Elastic fibers in dFB also developed postnatally, and they became less dense in the lower dermis with advancing age (Fig. S2A). By 2 years of age the dermis appeared thinner and *Col1a1* mRNA expression was low (Fig. 2A and S2D), the dWAT layer became devoid of AD, the dWAT showed extensive collagen staining (Fig. 2A and S2A). Together, these results show that age-dependent loss of adipogenic dFB is associated with a progressive loss in immature dermal fat and gain of fibrotic features.

To define adipogenic potential of the cells associated with the age related changes observed in mouse skin, dFB were isolated from skin at various ages and were differentiated into

adipocytes in vitro. While uncommitted embryonic E14 dFB were only partially adipogenic, neonatal P1 dFB were highly adipogenic and this adipogenic potential gradually declined during postnatal development (3 weeks~2 months) and was lost in aged 1 year dFB (Fig. 2F). Time course analysis of differentiating neonatal dFB showed that immature AD with small lipid droplets were formed as early as 2 days post differentiation (*p.d.*), and by day 4~7 *p.d.* >90% of cells became mature AD with large lipid droplets (Fig. 2G). Gene expression analyses revealed four distinct expression kinetics: (1) *Col1a1* and *Thy1* mRNA expression was highest in undifferentiated cells and gradually decreased as cells converted toward AD; (2) *Pdgfra*, *Sca1*, *Pref1* or *Pparg1* mRNA expression was detected prior to differentiation and were further elevated on day 1~2 *p.d.* followed by a robust decrease at day 4 *p.d.*; (3) *Camp* expression was induced as early as day 1 p.d. and peaked around day 2 *p.d.*; (4) *Pparg2*, *Adipoq* or *Fabp4* mRNA expression was induced later around day 2~4 *p.d.* and continued to increase as adipocytes matured (Fig. 2H–I). *Camp*$^{f/f}$*Pdgfra-cre* dFB or *Camp*$^{f/f}$*Adipoq-cre* dFB showed loss of *Camp* expression and secretion through differentiation *in vitro* (Fig. S2E–G), confirming that these adipose precursor cells are the major cellular source for cathelicidin. The ability of differentiating neonatal dFB to express *Camp* and *Pparg2* mRNA (Fig. 2J and S2H) and to secrete cathelicidin protein into conditioned medium (Fig. S2I–J) was progressively lost in dFB isolated from 3 weeks, 2 months and 1 year skin. In contrast, adult dFB produced higher *Col1a1* mRNA expression during differentiation (Fig. 2J), suggesting that decreased adipogenic function is accompanied by increased fibrogenic function in adult dFB. Functionally, the supernatant from differentiating P1 dFB potently inhibited the growth of *S. aureus* (SA113 and USA300) (Fig. 2K), whereas the age-related decline in antimicrobial protein expression correlated with decreased capacity of differentiating dFB to inhibit the growth of *S. aureus* (Fig. 2L–M). Therefore, taken together, these data show a loss of immature dermal fat and the adipogenic-antimicrobial function of dFB occurs with age.

Activation of the TGFβ pathway is associated with the loss of antimicrobial function of dFB

To better understand the change in antimicrobial and adipogenic function of dFB, we profiled the transcriptomes of primary dFB isolated at different ages by RNA-sequencing (RNA-seq). Because fibroblast populations become heterogeneous during postnatal development (Driskell et al., 2013) (Fig. S3A), Sca1$^+$ dFB were sorted from all postnatal groups to focus on the dFB population committed to the adipose lineage. Sca1 labeling purity was confirmed by flow cytometry (Figure S3B), and sorted Sca1$^-$ dFB were confirmed to be unable to differentiate into AD compared to Sca1$^+$ dFB (Fig. S3C). Because dFB lost their adipogenic function by 2 months of age (Fig. 2E), we chose 2 months as the most advanced age group for RNA-seq analyses.

Principle component analysis revealed a distinction in the transcriptomes of dFB isolated from different age groups. Embryonic E14 dFB and 2 month Sca1$^+$ dFB samples were clearly separated from P1 Sca1$^+$ dFB (Fig. 3A). Time course analyses identified seven gene clusters with multiple Gene Ontologies (GOs) undergoing distinct temporal changes (Fig. 3B and S3D–I). To identify top putative regulators that drive these age-associated changes, we performed Ingenuity Pathway Analysis (IPA) and identified TGFβ signaling as the top activated signaling pathway in 2 month Sca1$^+$ dFB compared to P1 Sca1$^+$ dFB (Fig. 3C).

IPA also predicted that TGFβ signaling activities were significantly altered in dFB from other age groups compared to P1 Sca1$^+$ dFB (Fig. S3J–K). Consistently, RNA-seq and RTqPCR analyses (Fig. 3D–G) revealed that the expression of the key genes in the TGFBR pathway, including *Tgfbr1 or Tgfbr2, Tgfb1 or Tgfb2* and *Inhba,* was elevated in 2 months compared to P1 Sca1+ dFB. Several TGFβ pro-fibrotic genes downstream of TGFβ including *Acta2* (gene coding for alpha smooth muscle actin-SMA), *Ctgf*, *Spp1, Pai1, Mmp13, Saa3 and Il6* were strongly elevated in 2 month cells compared to P1 cells. In contrast, the expression of several pro-adipogenic genes including *Pref1*, *Pparg, Sca1, Lpl* (Gregoire et al., 1998) and *Dcn* (a natural inhibitor of TGFβ signaling (Border et al., 1992)) was suppressed in 2 month cells compared to P1 cells. Similar to 2 month cells, embryonic E14 fibroblasts expressed and secreted significantly higher amounts of *Tgfb2* transcript and TGFβ2 protein, respectively (Fig. 3E–F). The expression of proadipogenic genes, including *Pparg*, *Sca1* and *Dcn* was suppressed in E14 compared to P1 cells, but profibrotic genes including *Acta2* and *Spp1* were only moderately elevated in E14 cells, suggesting that pro-fibrotic effect of TGFβ is preferentially suppressed in embryonic cells. Together, these results indicated that TGFβ could play a role in the age-related pro-adipogenic to pro-fibrotic switch of dFB.

TGFβ2 drives loss of adipogenic-antimicrobial function in neonatal dFB

To determine if the presence of TGFβ ligands were functionally relevant, neonatal dFB were treated with recombinant mouse TGFβ2. TGFβ2, as low as 0.1 ng/mL, potently suppressed the adipogenic function of P1 cells, and at higher doses (3~10 ng/mL) it not only completely abolished adipogenic function but also triggered a fibrotic phenotype, characterized by extensive cell striation and spindle-shaped morphology (Fig. 4A). In parallel, the induction of adipocyte marker genes, secretion of cathelicidin and FABP4 proteins, as well as suppression of *Col1a1* mRNA upon adipocyte differentiation was inhibited by TGFβ2 (Fig. 4B–C). In undifferentiated P1 dFB, TGFβ2 triggered a dose-dependent decrease in the expression of pro-adipogenic genes (*Sca1, Pref1, Pparg1 and Dcn)* and an increase in the expression of pro-fibrotic and inflammatory genes (*Spp1, Acta2, Mmp13, Pai1, Ctgf* and *Il6*) (Fig. 4D–E). Similar results were also seen in neonatal dFB treated with TGFβ1, except that TGFβ1 was 3~10 times less potent than TGFβ2 (Fig. S4A–B).

To characterize the dynamic interplay between pro-fibrotic and anti-adipogenic functions of TGFβ, Sca1 and SMA expression was evaluated in PDGFRA$^+$THY1$^+$ dFB by flow cytometry (Fig. S4C). Cultured neonatal PDGFRA$^+$THY1$^+$ dFB exhibited high Sca1 and low SMA mRNA expression. Treatment with TGFβ2 or TGFβ1 for 2 days led to a rapid dose-dependent decrease in Sca1 and increase in SMA expression (Fig. 4F–G and Fig. S4D). Flow cytometry analyses of cultured dFB from various ages revealed that while neonatal PDGFRA$^+$THY1$^+$ dFB were mostly Sca1^{hi}SMA^{lo}, dFB gradually lost Sca1 and gained SMA expression with age, and by 1 year most cells were Sca1^{lo}SMA^{hi} (Fig. 4H–I). Cultured 2 month or 1 year dFB strongly resembled neonatal dFB treated for 2 days with TGFβ2 (Fig. 4F). The antimicrobial activity of differentiating neonatal dFB against *S. aureus* was completely suppressed with addition of TGFβ2 (Fig. 4J–K and S4E). These results demonstrate that TGFβ2 is a potent suppressor of dFB's capacity to differentiate into AD and provide antimicrobial activity.

TGFβ exerts anti-adipogenic effects on dFB by activating the TGFBR-SMAD2,3 pathway

To understand the signaling pathway mediating the effect of TGFβ on dFB, downstream signaling molecules of the TGFβ pathway were evaluated. Phosphoblotting analyses of neonatal dFB treated with TGFβ2 showed that TGFβ2 induced a transient increase of SMAD2,3 and AKT phosphorylation (Fig. 5A). To determine the role of SMAD3 and AKT in the effects of TGFβ, small pharmacological inhibitors specific to SMAD3 (SIS3) (Jinnin et al., 2006), AKT (Wortmannin) (Zhang et al., 2016) or TGFBR (SB431542-SB) (Inman et al., 2002; Mordasky Markell et al., 2010) were applied. Pretreatment with either SMAD3 or TGFBR inhibitors, but not an AKT inhibitor, rescued TGFβ-driven suppression of *Pparg1* and induction of *Ctgf* mRNA expression (Fig. 5B), and restored the adipogenic function and the ability of neonatal dFB to produce and secrete cathelicidin (Fig. 5C–D and Fig. S5A). These results demonstrate that TGFβ exerts its pro-fibrotic and anti-adipogenic effects on dFB via the TGFBR-SMAD2,3 pathway.

Inhibition of TGFBR function boosts dFB adipogenic potential and enhances resistance to skin infection

To test the hypothesis that TGFβ2 is responsible for the age-dependent loss of adipogenic capacity of dFB, primary dFB isolated from mice of various ages were treated in culture for 3 days with a TGFBR inhibitor (SB). Inhibition of TGFBR reversed the loss of Sca1 and gain of SMA observed in $PDGFRA^{+}THY1^{+}$ dFB during aging (Fig. 5E–G). The age-associated suppression of pro-adipogenic *Pparg1* and increase of the pro-fibrotic *Spp1* were also reversed by SB treatment (Fig. 5H–I). Inhibition of TGFBR enabled embryonic and adult dFB to differentiate into mature adipocytes (Fig. 5J) and express cathelicidin (Fig. 5K). *Col1a1* expression was also suppressed upon TGFBR inhibition (Fig. S5B). Furthermore, the antimicrobial potential of the conditioned medium from differentiating embryonic dFB was enhanced when TGFBR was inhibited (Fig. 5L).

TGFβ signaling is active in the dermis and promotes loss of antimicrobial defense of mice

To investigate the role of the TGFβ pathway in dFB *in vivo*, activation of phosph-SMAD2,3 and the abundance of TGFβ was examined in mice of various ages. Increased pSMAD2,3 was seen in adult dermis (3 weeks~2 years) compared to neonatal dermis (Fig. 6A). P1 and 3 week skin showed random pSMAD2,3 distribution through the dermis while 2 month~2 year skin showed prominent pSMAD2,3 staining in the dWAT layer (Fig. 6A). This suggested that pSMAD2,3 signal may be preferentially turned on only in the committed pAd in dWAT during adulthood. Circulating TGFβ2 concentrations in serum were higher in neonatal (P1~P7) and young adult mice (3 weeks) but then declined progressively with advancing age (2 months~2 years) (Fig. 6B). In contrast, circulating TGFβ1 concentrations were lower in neonates and became elevated from adulthood through aging (Fig. 6C). To determine whether TGFβ may promote dermal fat loss in adulthood, adult mice were treated intradermally with TGFBR inhibitor (SB) for 5 days (Fig. 6D). SB-treated skin showed notable expansion of the dWAT layer (Fig. 6D) and higher expression of *Camp* and *Adipoq*, and lower expression of pro-fibrotic genes (*Col1a1* and *Ctgf*) (Fig. 6E).

To determine if these observations could translate into reduced susceptibility to infection *in vivo*, we administrated SB after infecting 1 year adult mouse skin with *S. aureus* strain

USA300 (Fig. 6F). Treating the infected mice with SB improved resistance to *S. aureus* skin infection as shown by a decrease in lesion size and bacterial CFU at both the infection edge and in the central area of the lesion (Fig.6F–G). RTqPCR analyses revealed that SB administration not only increased the expression of pAd or AD-related genes, including *Pdgfra* and *Camp,* but also suppressed expression of the pro-fibrotic gene *Spp1* at the infection site (Fig. 6H and S5C). Infection triggered adipocyte hyperplasia and cathelicidin protein production from dWAT that was enhanced in SB-treated mice (Fig. 6I). In addition, to inhibit TGFBR specifically in dFB, we generated conditional heterozygous deletion of *Tgfbr2* by crossing *Tgfbr2*$^{flox/flox}$ mice to *Pdgfra-cre* (*Tgfbr2*$^{flox/+}$*Pdgfra-cre*) (Fig. 6J). No homozygous *Tgfbr2*$^{flox/flox}$*Pdgfra-cre* offspring were generated despite extensive breeding, and thus experiments were only conducted with heterozygous offspring. dFB isolated from *Tgfbr2*$^{flox/+}$*Pdgfra-cre* mice expressed ~50% less *Tgfbr2* mRNA compared to WT dFB (Fig. S5D). *Tgfbr2*$^{flox/+}$*Pdgfra-cre* dFB were less responsive to exogenous TGFβ2 treatment as shown by an impaired induction of profibrotic genes including *Ctgf*, *Acta2* and *Spp1* (Fig. 6K–L). Importantly, when mice were subjected to *S. aureus* infection, the fibrotic response in the infected skin was significantly reduced in compared to WT control (Fig. 6M). Furthermore, more lipid droplets and cathelicidin protein were detected in the infected *Tgfbr2*$^{flox/+}$*Pdgfra-cre* dermis compared to infected WT controls (Fig. 6N). Overall bacterial abundance was lower, but not statistically significant, in the infected skin of *Tgfbr2*$^{flox/+}$*Pdgfra-cre* mice compared to WT controls (Fig. S5E–G), suggesting that heterozygous deletion of *Tgfbr2* in Pdgfra^{+} dFB may not be sufficient to drive a clinical phenotype. These changes demonstrate that TGFβ critically drives age-dependent loss of the innate antimicrobial function of the skin.

TGFβ promotes loss of adipogenic and antimicrobial defense function of primary human dermal fibroblasts

To determine if our observations in mice may also be relevant to humans, we evaluated dWAT in human skin samples (Caucasian; non-obese) from neonates (gestational week, GW 29~38), young adults (18 ~25 years), mid-age adults (50~65 years) and elderly donors (>75 years). Neonatal skin, either preterm (GW 29~32) or full term (GW 38~40), contained large volume of dWAT and thin a dermis, while in adulthood dWAT volume became gradually reduced and was eventually lost in mid-age and elderly skin samples (Fig. 7A and S6A). A similar trend of dWAT loss during adulthood was also observed in human skin biopsies (Chinese; non-obese) collected from young children (2~6 years), young adult (18~25 years) and mid-age adult (50~65 years) (Fig. S6B). Similar to mouse skin, the mRNA expression of *PREF1* or human cathelicidin *CAMP* was significantly higher in human neonatal skin compared to mid-age or elderly skin samples (Fig. 7B and S6C). Immunostaining of human skin sections for the human cathelicidin peptide LL-37 showed that it was abundantly expressed by neonatal dermal AD but not in the larger AD in aged skin (Fig. S6D). dWAT loss in adulthood coincided with an increase of dermal thickness, fibrogenesis as measured by collagen staining as well as *COL1A1* mRNA upregulation (Fig. 7A, S6A and S6E). In elderly human skin, similar to 2 year mouse skin, a decrease in dermal thickness, collagen content and *COL1A1* mRNA expression was observed (Fig. 7A, S6A and S6E), suggesting that prolong activation of dFB may eventually lead to loss of cells' profibrogenic function in elderly skin.

To determine if TGFβ can inhibit adipogenic function of human neonatal dFB, primary neonatal dFB isolated from 5 donors were differentiated into adipocytes with or without TGFBR inhibitor or recombinant TGFβ2. Neonatal dFB from three donors had high adipogenic capacity and highly expressed *CAMP* and *FABP4* mRNA, both of which could be completely inhibited with TGFβ2 treatment (Fig. S7A and Fig. 7C). In contrast, dFB isolated from the other two neonatal donors had low basal adipogenic capacity but became highly adipogenic and expressed high *CAMP* and *FABP4* mRNA when TGFBR inhibitor (SB) was added (Fig. S7A and Fig. 7C). Adipogenic capacity positively correlated with *PPARG* mRNA expression in undifferentiated cells prior to or after SB treatment (Fig. 7D).

To define the role of TGFβ in controlling the pro-adipogenic and pro-fibrotic functions of human dFB, we next focused on the neonatal dFB with low basal adipogenic capacity. Under basal conditions these cells had a notable fibrotic morphology, characterized by stratification and clustering of cells into aggregates (Fig. 7E), and this phenotype was further exacerbated upon treatment with TGFβ2, but was potently diminished upon treatment with SB (Fig. 7E). Flow cytometry analysis for SMA protein expression revealed that untreated cells were composed of mixed populations with low, medium and high expression of SMA, and TGFBR inhibitor treatment shifted these cell populations to mostly SMA^{lo} state, whereas TGFβ2 treatment shifted them toward mostly SMA^{hi} state (Fig. 7F). These cells expressed low basal *PPARG* mRNA and high *ACTA2* and *CTGF* (fibrotic gene) mRNA, and recombinant TGFβ2 further decreased *PPARG* and increased *ACTA2* and *CTGF* expression, whereas SB treatment strongly increased *PPARG* and almost completely suppressed *CTGF* expression (Fig. S7B–C). Thus, by default, these cells were weakly adipogenic, and TGFBR inhibitor treatment restored their adipogenic function and the ability to express *CAMP* (Fig. 7E and S7C). These results demonstrate that endogenous TGFβ pathway is constitutively active in neonatal human dFB with low basal adipogenic capacity, driving them to shift from a pro-adipogenic to a pro-fibrotic phenotype. Furthermore, antimicrobial assay using conditioned medium collected from undifferentiated and differentiated human neonatal dFB treated with SB demonstrated that only differentiating adipocytes treated with TGFBR inhibitor significantly suppressed growth of two *S. aureus* strains, including SA113 and USA300 (Fig. 7G). In addition, inhibition of TGFBR in primary adult dFB isolated from four mid-age adult donors also showed a significant decrease of mRNA expression for *CTGF* and *COL1A1* and an increase in *PPARG* (Fig. 7H), suggesting that TGFβ-mediated pro-adipogenic to pro-fibrotic switch also occurs in human adult cells. Together, these results are consistent with observations in mice and demonstrate that TGFβ drives loss of the adipogeni-cantimicrobial function of primary human dFB.

Discussion

Effective defense against *S. aureus* infections relies on proper immune response from skin resident cells including adipogenic dFB (Zhang et al., 2015), lymphoid and myeloid immune cells such as T lymphocytes, neutrophils and macrophages (Dillen et al., 2018; Feuerstein et al., 2015; Miller et al., 2006). It is well established that myeloid derived innate and adaptive immunity is deficient early in life (Futata et al., 2012; Georgountzou and Papadopoulos, 2017; Shaw et al., 2013), suggesting that the non-myeloid resident cells such as adipogenic dFB may provide critical host defense against invasive *S. aureus* infections, especially in

early life. However, age-related changes in the innate immune function of adipogenic dFB have been unexplored.

We have shown that PDGFRA^{+}THY1^{hi} dFB responded to infection by producing cathelicidin through reactive adipogenesis, and loss of this antimicrobial response led to increase of susceptibility to *S. aureus* infection. We have also shown that neonatal skin immunity was comprised of highly adipogenic PDGFRA^{+}THY1^{hi} dFB and large volume of immature dermal fat that highly expressed cathelicidin. These results suggest that adipogenic dFB and immature fat layer may function as critical antimicrobial protective components in neonatal skin immunity, when myeloid and lymphoid immune systems are not yet mature. During postnatal development and in adulthood, PDGFRA^{+}THY1^{hi} dFB population, immature fat and adipogenic potential of dFB became progressively lost as the myeloid immune system matured, suggesting that the latter is compensating for the loss of innate immune function of adipogenic dFB.

To identify the underlying mechanisms for age-dependent changes in adipogenic function of dFB, we cultured primary dFB isolated from mouse skin at different ages and observed a drastic pro-adipogenic to pro-fibrotic switch that was age-dependent: neonatal dFB were highly adipogenic and potently inhibited bacterial growth, whereas adult cells gained pro-fibrotic features and both embryonic and adult dFB had low adipogenic capacity and were not able to control bacterial growth. Based on RNA-seq analysis we hypothesized a key role for TGFβ and confirmed it by reproducing the phenotype of adult or aged cells following treatment of neonatal dFB with recombinant TGFβ2 protein, and by rescuing loss of function in embryonic or adult or aged dFB following administration of a pharmacological inhibitor of TGFBR or via targeted genetic deletion. Administration of TGFB inhibitor or targeted heterozygous deletion of *Tgfbr2* in Pdgfra^{+} dFB was also effective *in vivo* to restore the reactive adipogenesis-antimicrobial defense function of dFB in adult mice. Although the pro-fibrotic (Lakos et al., 2004) and anti-adipogenic functions (Choy and Derynck, 2003) of TGFβ pathway are already known, our results identify these fundamental functions of TGFβ as a key regulatory mechanism controlling the innate antimicrobial function of dFB.

In vitro, *Tgfb2* was the most abundant TGFβ isoform expressed by dFB, and its expression correlated with the age-related loss of adipogenic potential. TGFβ2 was found to be 3~10 times more potent than TGFβ1 in triggering adipogenic to pro-fibrotic switch in neonatal dFB. *In vivo*, circulating TGFβ2 concentrations in mouse serum were higher early in life (from P1~3 weeks) then declined from adulthood through aging, whereas circulating TGFβ1 concentrations were lower in neonates and became elevated with advancing age. We posit that high serum TGFβ2 early in life may drive rapid loss of adipogenic function of neonatal dFB during postnatal development, whereas decline in TGFβ2 serum concentration later in life may be compensated by rising TGFβ1. TGFβ2 can also be produced by other skin cell types such as hair follicle keratinocytes and dermal papilla cells (Hibino and Nishiyama, 2004; Soma et al., 2002), and TGFβ2 may synergize with TGFβ1, which is abundantly produced by immune cells such as macrophages (Keophiphath et al., 2009) and regulatory T cells (Bommireddy and Doetschman, 2007). Alternatively, endogenous production of TGFβ from adipocytes or surrounding stromal cells could provide a source for autocrine or

paracrine suppression of adipocyte progenitors. Future study will be needed to determine cellular source of these TGFβ ligands.

Dermal fibroblasts are the major mesenchymal cell type in the skin and these cells exhibit considerable functional diversity, which was also observed in our culture system. Primary mouse neonatal dFB culture appeared highly homogeneous (>90% of cells were $Sca1^{hi}SMA^{lo}$), whereas adult dFB appeared heterogeneous with mixed populations of $Sca1^{hi\text{-}lo}$ and $SMA^{lo\text{-}hi}$ cells in culture. The $Sca1^{lo}SMA^{hi}$ dFB harbored a myofibroblasts-like gene signature (Hinz et al., 2012; Lee et al., 2010), and exhibited high mRNA expression of pro-fibrotic genes (such as *Acta2*, *Ctgf* and *Spp1*) and low expression of pro-adipogenic expression (such as *Pref1* and *Pparg1*) compared to $Sca1^{hi}SMA^{lo}$ neonatal dFB. This adipogenic to pro-fibrotic switch by adult cells could be reversed upon inhibition of TGFBR, suggesting that the plasticity between distinct phenotypic subpopulations of dFB maybe controlled by TGFβ. Analogous two-way conversion between myofibroblasts and adipogenic fibroblasts has been reported in several recent studies using genetic lineage-tracing tools in mice. In the mouse model of idiopathic pulmonary fibrosis, lung lipogenic fibroblasts have been observed to differentiate into myofibroblasts during early fibrosis formation and later, during resolution of fibrosis, the population of newly formed myofibroblasts switches back to lipogenic fibroblasts (El Agha et al., 2017). In the skin, myofibroblasts that accumulate in the bleomycin-induced mouse model of scleroderma originate from Adipoq-positive intradermal progenitors (Marangoni et al., 2015). Furthermore, myofibroblasts formed during early skin wound healing give rise to new adipocytes that regenerate *de novo* during later stages of wound healing around *de novo* hair follicles (Plikus et al., 2017). Highly relevant to our work, these studies suggest that the pool of adipogenic fibroblasts in the skin or lung can switch between a pro-fibrotic phenotype (such as myofibroblasts) during injury and a pro-adipogenic phenotype during injury resolution. Our results here suggest that TGFβ maybe the key factor that regulates this plasticity between distinct phenotypic subpopulations of dFB. Future studies are needed to identify the endogenous inhibitor of TGFBR that converts pro-fibrotic dFB toward adipogenic lineage.

In conclusion, these observations have uncovered an age-dependent activation of TGFβ pathway that attenuates adipogenic function of dermal fibroblasts and promotes a subsequent loss of antimicrobial defense by dermal fat. This work provides insights into how activation of TGFβ negatively impacts skin defense against infection and suggests that small molecules that suppress TGFBR might be an effective therapeutic to combat skin infections.

STAR Methods

Animals and animal care

All animal experiments were approved by the University of California, San Diego (UCSD), Institutional Animal Care and Use committee. C57BL/6 wildtype mice were originally purchased from Jackson laboratory, and were then breeded and maintained in animal facility of UCSD. For aging mouse model, dorsal skin biopsies were collected from C57BL/6 wildtype male mice with various ages (E14, P1, 3W, 2 months and 1 year old). *Pdgfra-cre* mice (Stock No: 013148), *Adipoq-cre* mice (Stock No: 028020) and $Tgfbr2^{flox/flox}$ mice

(Stock No: 012603) were originally purchased from Jackson laboratory then breeded and maintained in animal facility of UCSD. *Camp*$^{flox/flox}$ mice, in which exon 2 and exon 4 of Camp gene were flanked by LoxP sites, were generated by Ozgene (Bentley DC, WA, Australia) Fibroblasts or adipocyte specific deletion of *Camp* were generated by breeding *Camp*$^{flox/flox}$ mice with *Pdgfra-cre* mice or *Adipoq-cre* mice respectively. *Tgfbr2* specific deletion in fibroblasts was achieved by breeding *Tgfbr2*$^{flox/flox}$ mice with *Pdgfra-cre* mice. Probably due to early embryonic lethality, we were not able to get the homozygous deletion of *Tgfbr2* in fibroblasts (*Tgfbr2*$^{flox/flox}$;*Pdgfra-cre)* over more than one year of breeding, so the heterozygous deletion of *Tgfbr2* in fibroblasts (*Tgfbr2*$^{flox/+}$;*Pdgfra-cre)* was used instead as the *Tgfbr2* heterozygous deletion model to study the role of TGFBR pathway in the infection triggered dermal adipogenesis-antimicrobial response. Dorsal skin biopsies around the same area were collected from mice with various ages for analysis to control the consistency of the tissue site collected over the whole lifetime of the mouse

Mouse model of S. aureus skin infection

Skin infection experiments were done as described before (Zhang et al., 2015). *Staphylococcus aureus* strain USA300 (MRSA) was used for in vivo infection. In brief, the backs of sex-matched and age-matched adult wildtype or indicated strain of mutant mice were shaved and hair removed by chemical depilation (Nair) then injected subcutaneously with 100 μL of a mid-logarithmic growth phase of S. aureus (1×10^7 CFU of bacteria) in PBS. Mice were sacrificed after day 3 and skin biopsy covering the infection area was harvested. Skin biopsies were homogenized in 1 mL Trizol (for RNA) or PBS (for CFU counting) with 2 mm zirconia beads in a mini-bead beater 16 (Biospect, Bartlesville, OK). To count CFU, homogenized skin samples were serially diluted, plated onto Tryptic Soy Agar, and enumerated after 18 hrs to quantify the CFU per gram of tissue. For administration of TGFBR inhibitor, SB431542 (0.125 mg in 100uL of 2% DMSO + 30% PEG300 + PBS) or vehicle control was injected intradermally within the infection site at 24 hrs and 48 hrs post infection and skin biopsies were collected at day 3 post infection for RNA extraction or CFU count as described above. For all animal studies, animals were randomly selected without formal pre-randomization and quantitative measurements were done without the opportunity for bias.

Chemicals, antibodies and dyes

IBMX (3-Isobutyl-1-methylxanthine), dexamethasone, indomethacin, and recombinant human insulin were purchased from Sigma-Aldaich (St. Louis, MO). SB431542 and SIS3 were purchased from Selleckchem (Houston, TX). Wortmannin was purchased from EMD Millipore (Billerica, MA). Rabbit anti-CRAMP and rabbit anti-LL-37 antibodies were made from our lab as described previously (Zhang et al., 2015; Zhang et al., 2016); goat anti-COLIV, mouse anti-FABP4 and rabbit anti-SMAD2,3 antibodies are from Abcam (Cambridge, MA); Lipid dye bodipy is from Molecular Probes (Eugene, OR). Rabbit anti-Phospho-SMAD2, 3, rabbit anti-phospho-AKT antibody and mouse anti-AKT antibody were purchased from Cell Signaling (Danvers, MA). Recombinant mouse TGFβ1 and TGFβ2 were purchased from R&D Systems (Minneapolis, MN).

Human skin sample collection

Fresh adult human (Caucasian) full thickness skin biopsies, from the back of healthy and non-obese male donors between 18~90 years of age, were collected by the Dermatology clinics, University of California San Diego. Fresh adult human (Chinese) full thickness skin biopsies were collected by Hospital for skin disease, Institute of Dermatology, Chinese Academy of Medical Science and Peking Union Medical College. All sample acquisitions, were approved and regulated by the University of California San Diego Institutional Review Board (reference number 140144) or by Institute of Dermatology, Chinese Academy of Medical Science Medical Ethics Committee (reference number 2012003). The informed consent was obtained from all subjects prior to skin biopsies. Fresh neonatal full thickness skin samples, from the back of neonatal donors, were obtained from the international institute for advancement of Medicine (IIAM; Exton, PA). The informed consent was obtained from parent of neonatal donor prior to skin collection. All human biopsies were taken from the back skin, where it is relatively protected from sun exposure compared to other regions such as face and neck of the body. Upon collection, these samples were directly fixed with PFA then proceed for either paraffin embedding or OCT embedding for histological or immunofluorescent analyses.

Histology, collagen trichrome staining and immunohistochemistry (IHC)

Paraffin embedding and sectioning was performed by the Moores cancer center histology core at UCSD. For OCT embedding, tissue biopsies were first fixed with 4% PFA for 2 hours then cryoprotected by sucrose for 48 hours prior to being embedded in OCT compound and stored in −80 ^{O}C. Histological analysis was performed using either paraffin sections or frozen sections by Hematoxylin-Eosin (H&E) staining. Collagen was stained by the Richard-Allan Scientific Gomori Trichrome green collagen staining kit (ThermoFisher Scientific, Waltham, MA, USA). Elastic staining (Thermo Fisher Scientific, Waltham, MA, USA) and hydroxyproline assay (BioVision) were performed on human or mouse tissues according to manufacturer's instructions. For IHC, fixed and permeabilized tissue sections were blocked with Image-iT FX reagent (invitrogen) before incubating with primary antibodies followed by appropriate 488- or Cy3-coupled secondary antibodies. Nuclei were counter-stained with DAPI. All images were taken with an Olympus BX41 microscope (widefield) or Zeiss LSM510 confocal microscope as indicated.

Primary dermal fibroblast isolation and culture

For neonatal mouse dorsal skin, epidermis was first removed from the dermis by overnight dispase digestion as described before (Li et al., 2017), and for adult skin hair was first removed by clipper then cut into 5mm wide strips prior to dispase digestion. The dermis was then cut into small pieces (~1 mm) by scalpel then digested with 2.5 mg/mL Collagenase D and 30 ng/mL DNAse1 for 2 hours at 37 ^{O}C with constant rocking to release dermal fibroblasts. Cells mixture was then filtered through 30 μm filter into single cell suspension then treated with red blood cell lysis buffer. Isolated dermal fibroblasts were cultured in growth medium (DMEM supplemented with 10% FBS, glutamax and antibiotics-antimicotics) in a humidified incubator at 5% CO2 and 37°C under sterile conditions. Fresh medium was replenished daily to remove debris or dead cells. Primary cells were then

trypsinized within 3 days and replated at 5×10^4/mL for in vitro assays, and only passage 1 cells were used for experiment. To induce adipocyte differentiation, two day post-confluent dFB were switched to adipocyte differentiation medium containing 2 μM Dexamethasone, 250 μM IBMX, 200 μM Indomethacin and 10 μg/mL recombinant human insulin. Fresh differentiation medium was changed at day 2, 4, and 7 during the differentiation time course.

Flow cytometry and analysis (FACS)

FACS analysis of primary dermal fibroblasts was modified from previously reported method for adipogenic fibroblasts (Chia et al., 2016; Rivera-Gonzalez et al., 2016). Briefly, freshly isolated dFB from mouse skin or primary cultured of dFB first were stained with zombie violet viability dye (BioLegend, 423114) to stain dead cells. Cells were then blocked with anti-mouse CD16/32 (eBioscience, 14016185), followed by staining with an antibody cocktails containing PECy7-CD45 (BioLegend, 147704), PerCP-Cy5.5-CD31 (BioLegend, 102522), PE-THY1 (BioLegend, 105308), APC-PDGFRA (CD140a) (eBioscience, 17140181) and BV605-Sca1 (BioLegend, 108133). Stained cells were then fixed and permeabilized using the intracellular fixation and permeabilization buffer set (eBioscience), then intracellular SMA was stained by AF488-SMA (eBioscience, 53976082). For FACS staining of T cell populations, cells were stained with an antibody cocktail including APC-CD4 (Biolegend, 100516), BV510-CD8a (Biolegend, 100752), APC-Cy7-TCRβ (Biolegend, 12–5711-82), PE-TCRδγ (eBioscience, 12–5711-82), and PerCP-Cy5.5-CD45.2 (Biolegend, 109828). For FACS staining of other myeloid immune cell panel, cells were stained with an antibody cocktail including PECy7-CD11B (BioLegend, 101216), FITC-Ly6G (eBioscience, 11593182), PE-F4/80 (eBioscience,12480182), APC-CD11C (BioLegend, 117310), AF700-MHCII and (eBioscience, 56532182) FACS analysis for protein expression of each cell marker was performed by the BD FACSCanto RUO machine and analyzed by FlowJo V10 software. Dead cells stained positive with zombie violet dye were excluded from the analyses.

Reverse transcription-quantitative PCR (RTqPCR) analyses

Total cellular RNA was extracted using the PureLink RNA isolation kit with RNase-free DNase1 digestion to remove genomic DNA contamination (Qiagen) and 500 ng of RNA was reverse transcribed to cDNA using iScript cDNA synthesis kit (Bio-rad). Quantitative, real-time PCR was performed on the CFX96 real time system (Bio-rad) using SYBR Green Mix (Bimake, Houston, Tx). All of the primers used with SYBR green were designed to span at least one exon to minimize the possibility of nonspecific amplification from the genomic DNA. The expression of *Tbp* gene (TATA-Box Binding Protein) was used as a house keeping gene to normalize data for the expression of mouse genes, and *HPRT* was used as a house keeping gene for the expression of human genes. Specific primer sequences are shown in supplementary Table S1 (mouse genes) and Table S2 (human genes).

Immunoblotting analyses

10ul of cell medium was separated on a 10–20% Tris-Tricine precast gel (Biorad), transferred to PVDF membrane (Biorad), followed by immunoblotting using indicated primary antibodies followed by fluorescent secondary antibodies (LICOR) and imaging using fluorescent Odyssey System (LICOR).

TGFβ1 and TGFβ2 ELISA

Mouse TGFβ1 or TGFβ2 ELISA Kit was purchased from R&D Systems (Minneapolis, MN) and TGFβ1 orTGFβ2 concentrations in conditioned medium from primary mouse dermal fibroblasts or mouse serum were determined according to manufacturer's instruction.

In vitro bacterial killing assay

Antibiotic free and phenol-red free conditioned medium was collected from differentiating dermal fibroblasts as described before (Zhang et al., 2015). The conditioned medium (100 μL) was then mixed with 10^5/ml CFU (colony forming unit) of indicated bacterial strain in 96 well tissue culture microtiter plates and incubated at 37°C for 10 ~48 hrs prior to plating for CFU counting. The optical density at 595 nm (OD595) was also measured every 2~4 hours by a spectrometer.

Sample preparation for RNA-seq

Primary dermal fibroblasts, isolated from dorsal skin of mouse at E14, E17, P1, 3 weeks and 2 months of age, were harvested at the first passage. To enrich fibroblasts that have committed to adipocyte lineage, Sca1+ dFB were purified from P1, 3 week and 2 month dFB using the anti-Sca1 microbeads kit and MACS columns and separators (Miltenyi Biotec, San Diego, CA). Purity of cells from each age group was greater than 90% as confirmed by FACS analyses. Total cellular RNA was extracted using the PureLink RNA isolation kit with DNase1 digestion to remove genomic DNA contamination (Life Technologies) and 10 ng total RNA (n=3 for each age group) was used for SMART-seq2.

SMART-seq2

SMART-seq2 was performed as previously described with minor modifications (Picelli et al., 2013; Picelli et al., 2014). Briefly, 10 ng total RNA (RIN >9.6) was reversed transcribed using Super Script II (Invitrogen). cDNA was pre-amplified for 10 cycles using high fidelity KAPA HiFi HotStart Ready Mix (Kapa Biosystems). Pre-amplified cDNAs were cleaned with AMPure XP beads (Beckman Coulter) at a 1:1 ratio and eluted with elution buffer (Qiagen). Tn5-mediated tagmentation was performed on 18 ng total cDNA using the Nextera DNA Sample Preparation Kit (Illumina) at 55°C for 5 minutes and deactivated with PM buffer (Qiagen). Adapter-ligated fragments were amplified for 8 continuous cycles using universal Ad1 and unique Ad2.xx barcodes (IDT). Amplified PCR fragments were purified with AMPure XP beads as suggested (Beckman Coulter). Size selected libraries were quantified using Qubit (Thermo), loaded on a High-Sensitivity DNA chip for quality control (Agilent), and quantified using KAPA for Illumina Sequencing Platforms (Illumina). Libraries were multiplexed and sequenced as paired-end, 43 bps on a NextSeq 500 Illumina Sequencing Platform (Illumina) (Cluster density = 252K/mm2, Clusters PF = 78.8%, Q30 = 90.7%).

Transcript alignment, quantification and filtering

Paired-end reads were aligned to the mouse genome (mm10/gencode.vM4) with bowtie (version 1.0.0) and quantified using the RNA-seq by Expectation-Maximization algorithm (RSEM) (version 1.2.12) with the following standard parameters: *rsem-calculate-expression*

-p $CORES --paired-end (Li and Dewey, 2011). Samples displaying >12,000,000 aligned reads and >77% alignment were considered for downstream analyses. Samples were filtered and only protein-coding genes and lncRNAs expressed at minimum 1 TPM in at least one sample in all biological replicates were considered for downstream analyses.

SMART-seq2 and IPA analyses

Differential expression dynamics across E14, E17, P1-*Sca1*$^{+}$, 3W-*Sca1*$^{+}$, 2M-*Sca1*$^{+}$ samples was identified using the single-time series, two-step regression model algorithm Next maSigPro using with the following parameters under the T.Fit, get.siggenes and see.genes functions: *alfa = 0.01, vars="all", rsq = 0.7, k=7* (Nueda et al., 2014). Principle component analyses were performed using the R ggbiplot package. Pathway and upstream regulator analyses were performed by Ingenuity pathway analysis (IPA) from Qiagen.

Statistics

Experiments were repeated at least 3 times with similar results. Statistical significance was determined using Student's unpaired two-tailed t-test, or one way ANOVA multiple comparison test as indicated in the legend (*P<0.05, **P<0.01, ***P<0.001, ****P<0.0001).

Supplementary Material

Refer to Web version on PubMed Central for supplementary material.

Acknowledgments

This work was supported by NIH grant R01AR069653 to Drs. L.Z. and R.L.G., NIH R01 AI083358, R01 AR052728 and U19 AI117673 to RLG. M.V.P. is supported by Pew Charitable Trust grant and NIH grants U01 AR073159, R01 AR067273, NSF Grant DMS1763272, and Simons Foundation Grant (594598, QN). C.F.G.J. is supported by NSF-GRFP (DGE-1321846) and MBRS-IMSD training grant (GM055246). Y.Z. is supported by NIH R01 AI107027. We thank UCSD flow cytometry core for flow cytometry studies and Professor Pier Lorenzo Puri for comments on the manuscript.

References

Bommireddy R, and Doetschman T (2007). TGF beta 1 and T(reg) cells: alliance for tolerance. Trends Mol Med 13, 492–501. [PubMed: 17977791]

Border WA, Noble NA, Yamamoto T, Harper JR, Yamaguchi Y, Pierschbacher MD, and Ruoslahti E (1992). Natural inhibitor of transforming growth factor-beta protects against scarring in experimental kidney disease. Nature 360, 361–364. [PubMed: 1280332]

Chia JJ, Zhu T, Chyou S, Dasoveanu DC, Carballo C, Tian S, Magro CM, Rodeo S, Spiera RF, Ruddle NH, et al. (2016). Dendritic cells maintain dermal adipose-derived stromal cells in skin fibrosis. J Clin Invest 126, 4331–4345. [PubMed: 27721238]

Choy L, and Derynck R (2003). Transforming growth factor-beta inhibits adipocyte differentiation by Smad3 interacting with CCAAT/enhancer-binding protein (C/EBP) and repressing C/EBP transactivation function. The Journal of biological chemistry 278, 9609–9619. [PubMed: 12524424]

Dillen CA, Pinsker BL, Marusina AI, Merleev AA, Farber ON, Liu HY, Archer NK, Lee DB, Wang Y, Ortines RV, et al. (2018). Clonally expanded gamma delta T cells protect against Staphylococcus aureus skin reinfection. J Clin Invest 128, 1026–1042. [PubMed: 29400698]

Driskell RR, Lichtenberger BM, Hoste E, Kretzschmar K, Simons BD, Charalambous M, Ferron SR, Herault Y, Pavlovic G, Ferguson-Smith AC, et al. (2013). Distinct fibroblast lineages determine dermal architecture in skin development and repair. Nature 504, 277-+. [PubMed: 24336287]

El Agha E, Moiseenko A, Kheirollahi V, De Langhe S, Crnkovic S, Kwapiszewska G, Szibor M, Kosanovic D, Schwind F, Schermuly RT, et al. (2017). Two-Way Conversion between Lipogenic and Myogenic Fibroblastic Phenotypes Marks the Progression and Resolution of Lung Fibrosis (vol 20, pg 261, 2017). Cell stem cell 20, 571–571.

Festa E, Fretz J, Berry R, Schmidt B, Rodeheffer M, Horowitz M, and Horsley V (2011). Adipocyte Lineage Cells Contribute to the Skin Stem Cell Niche to Drive Hair Cycling. Cell 146, 761–771. [PubMed: 21884937]

Feuerstein R, Seidl M, Prinz M, and Henneke P (2015). MyD88 in macrophages is critical for abscess resolution in staphylococcal skin infection. Journal of immunology 194, 2735–2745.

Futata EA, Fusaro AE, de Brito CA, and Sato MN (2012). The neonatal immune system: immunomodulation of infections in early life. Expert Rev Anti-Infe 10, 289–298.

Georgountzou A, and Papadopoulos NG (2017). Postnatal innate immune Development: From Birth to Adulthood. Front Immunol 8.

Gregoire FM, Smas CM, and Sul HS (1998). Understanding adipocyte differentiation. Physiol Rev 78, 783–809. [PubMed: 9674695]

Hibino T, and Nishiyama T (2004). Role of TGF-beta2 in the human hair cycle. Journal of dermatological science 35, 9–18. [PubMed: 15194142]

Hinz B, Phan SH, Thannickal VJ, Prunotto M, Desmouliere A, Varga J, De Wever O, Mareel M, and Gabbiani G (2012). Recent developments in myofibroblast biology: paradigms for connective tissue remodeling. Am J Pathol 180, 1340–1355. [PubMed: 22387320]

Inman GJ, Nicolas FJ, Callahan JF, Harling JD, Gaster LM, Reith AD, Laping NJ, and Hill CS (2002). SB-431542 is a potent and specific inhibitor of transforming growth factor-beta superfamily type I activin receptor-like kinase (ALK) receptors ALK4, ALK5, and ALK7. Mol Pharmacol 62, 65–74. [PubMed: 12065756]

Jinnin M, Ihn H, and Tamaki K (2006). Characterization of SIS3, a novel specific inhibitor of Smad3, and its effect on transforming growth factor-beta1-induced extracellular matrix expression. Mol Pharmacol 69, 597–607. [PubMed: 16288083]

Kasza I, Suh Y, Wollny D, Clark RJ, Roopra A, Colman RJ, MacDougald OA, Shedd TA, Nelson DW, Yen MI, et al. (2014). Syndecan-1 Is Required to Maintain Intradermal Fat and Prevent Cold Stress. Plos Genet 10.

Keophiphath M, Achard V, Henegar C, Rouault C, Clement K, and Lacasa D (2009). Macrophage-secreted factors promote a profibrotic phenotype in human preadipocytes. Molecular endocrinology 23, 11–24. [PubMed: 18945811]

Kirkland JL, Hollenberg CH, and Gillon WS (1993). Ageing, differentiation, and gene expression in rat epididymal preadipocytes. Biochemistry and cell biology = Biochimie et biologie cellulaire 71, 556–561. [PubMed: 8192892]

Klein E, Smith DL, and Laxminarayan R (2007). Hospitalizations and deaths caused by methicillin-resistant Staphylococcus aureus, United States, 1999–2005. Emerging infectious diseases 13, 1840–1846. [PubMed: 18258033]

Lakos G, Takagawa S, Chen SJ, Ferreira AM, Han G, Masuda K, Wang XJ, DiPietro LA, and Varga J (2004). Targeted disruption of TGF-beta/Smad3 signaling modulates skin fibrosis in a mouse model of scleroderma. Am J Pathol 165, 203–217. [PubMed: 15215176]

Lee CH, Shah B, Moioli EK, and Mao JJ (2010). CTGF directs fibroblast differentiation from human mesenchymal stem/stromal cells and defines connective tissue healing in a rodent injury model. J Clin Invest 120, 3340–3349. [PubMed: 20679726]

Marangoni RG, Korman BD, Wei J, Wood TA, Graham LV, Whitfield ML, Scherer PE, Tourtellotte WG, and Varga J (2015). Myofibroblasts in Murine Cutaneous Fibrosis Originate From Adiponectin-Positive Intradermal Progenitors. Arthritis Rheumatol 67, 1062–1073. [PubMed: 25504959]

Miller LS, and Cho JS (2011). Immunity against Staphylococcus aureus cutaneous infections. Nat Rev Immunol 11, 505–518. [PubMed: 21720387]

Miller LS, O'Connell RM, Gutierrez MA, Pietras EM, Shahangian A, Gross CE, Thirumala A, Cheung AL, Cheng GH, and Modlin RL (2006). MyD88 mediates neutrophil recruitment initiated by

IL-1R but not TLR2 activation in immunity against Staphylococcus aureus. Immunity 24, 79–91. [PubMed: 16413925]

Mordasky Markell L, Perez-Lorenzo R, Masiuk KE, Kennett MJ, and Glick AB (2010). Use of a TGFbeta type I receptor inhibitor in mouse skin carcinogenesis reveals a dual role for TGFbeta signaling in tumor promotion and progression. Carcinogenesis 31, 2127–2135. [PubMed: 20852150]

Philippeos C, Telerman SB, Oules B, Pisco AO, Shaw TJ, Elgueta R, Lombardi G, Driskell RR, Soldin M, Lynch MD, et al. (2018). Spatial and Single-Cell Transcriptional Profiling Identifies Functionally Distinct Human Dermal Fibroblast Subpopulations. The Journal of investigative dermatology 138, 811–825. [PubMed: 29391249]

Plikus MV, Guerrero-Juarez CF, Ito M, Li YR, Dedhia PH, Zheng Y, Shao M, Gay DL, Ramos R, Hsi TC, et al. (2017). Regeneration of fat cells from myofibroblasts during wound healing. Science 355, 748–752. [PubMed: 28059714]

Rivera-Gonzalez GC, Shook BA, Andrae J, Holtrup B, Bollag K, Betsholtz C, Rodeheffer MS, and Horsley V (2016). Skin Adipocyte Stem Cell Self-Renewal Is Regulated by a PDGFA/AKT-Signaling Axis. Cell stem cell 19, 738–751. [PubMed: 27746098]

Schmidt BA, and Horsley V (2013). Intradermal adipocytes mediate fibroblast recruitment during skin wound healing. Development 140, 1517–1527. [PubMed: 23482487]

Shaw AC, Goldstein DR, and Montgomery RR (2013). Age-dependent dysregulation of innate immunity. Nat Rev Immunol 13, 875–887. [PubMed: 24157572]

Soma T, Tsuji Y, and Hibino T (2002). Involvement of transforming growth factor-beta2 in catagen induction during the human hair cycle. The Journal of investigative dermatology 118, 993–997. [PubMed: 12060393]

Sun K, Tordjman J, Clement K, and Scherer PE (2013). Fibrosis and Adipose Tissue Dysfunction. Cell Metab 18, 470–477. [PubMed: 23954640]

Tabib T, Morse C, Wang T, Chen W, and Lafyatis R (2018). SFRP2/DPP4 and FMO1/LSP1 Define Major Fibroblast Populations in Human Skin. The Journal of investigative dermatology 138, 802–810. [PubMed: 29080679]

Zhang LJ, Guerrero-Juarez CF, Hata T, Bapat SP, Ramos R, Plikus MV, and Gallo RL (2015). Dermal adipocytes protect against invasive Staphylococcus aureus skin infection. Science 347, 67–71. [PubMed: 25554785]

Zhang LJ, Sen GL, Ward NL, Johnston A, Chun K, Chen YF, Adase C, Sanford JA, Gao NN, Chensee M, et al. (2016). Antimicrobial Peptide LL37 and MAVS Signaling Drive Interferon-beta Production by Epidermal Keratinocytes during Skin Injury. Immunity 45, 119–130. [PubMed: 27438769]

Zwick RK, Guerrero-Juarez CF, Horsley V, and Plikus MV (2018). Anatomical, Physiological, and Functional Diversity of Adipose Tissue. Cell Metab 27, 68–83. [PubMed: 29320711]

Highlights

1. Neonatal skin is enriched with immature fat and adipogenic dermal fibroblasts
2. Dermal immature fat and the adipogenic-antimicrobial dFB are lost with age
3. TGFβ pathway promotes the age-related adipogenic to fibrotic switch of dFB
4. Inhibition of TGFBR restores antimicrobial function of dFB in adult mice

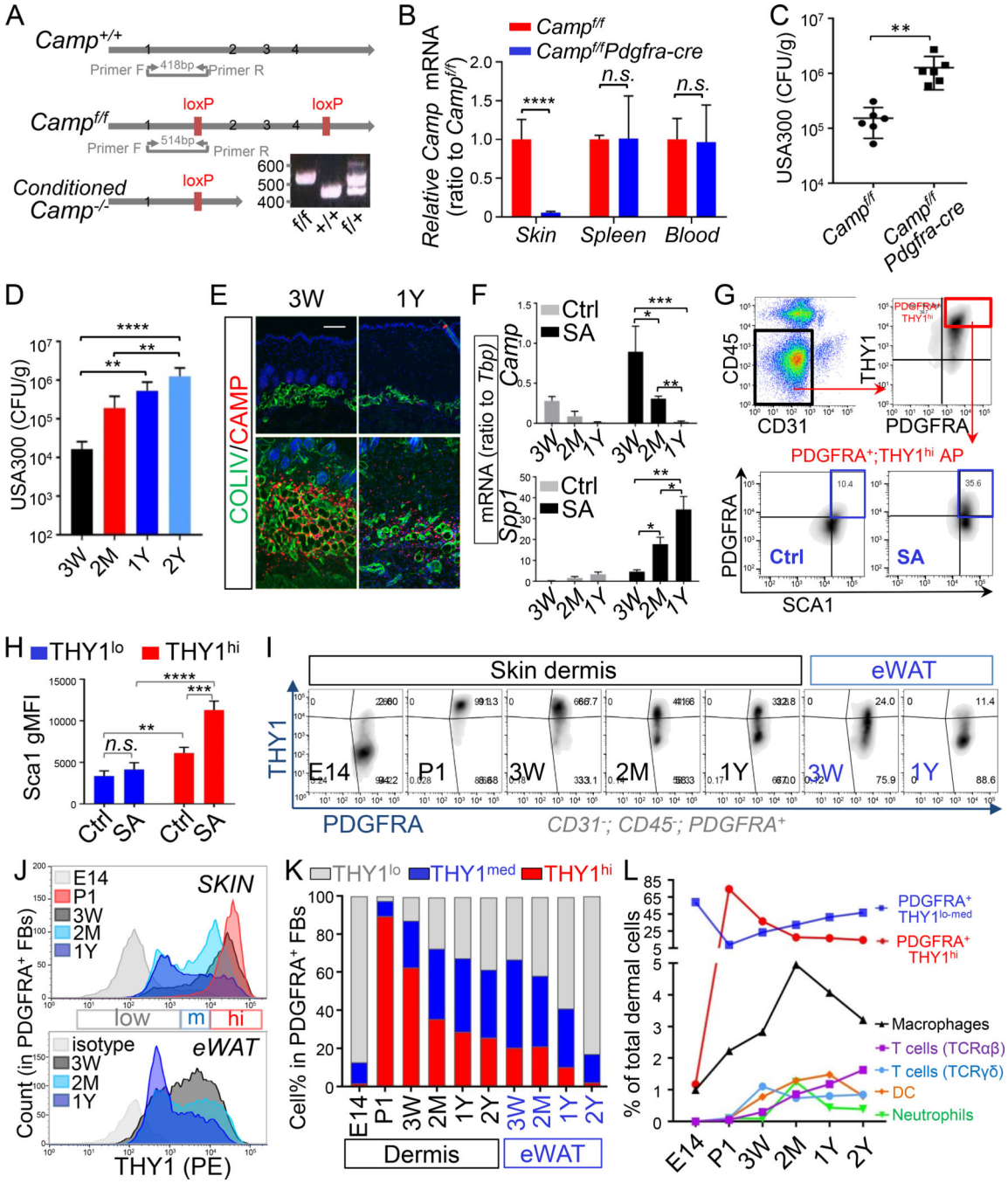

Figure 1. Dermal PDGFRA^{+}THY1^{hi} adipocyte progenitors and their antimicrobial response are lost with advancing age.

(**A**). Schematic representation of the mouse *Camp* locus with exons 2~4 flanked by LoxP sites. Insert gel image represents genotyping result of wildtype (+/+), heterozygote (f/+) and homozygous mutant (f/f) mice using primers flanking *Camp* gene as indicated. (**B**). *Camp*$^{f/f}$ (WT) or *Camp*$^{f/f}$*Pdgfra-cre* (*Camp*$^{f/f}$;*Pdgfra-cre*) littermate mice (2 month of age) were infected intradermally (*i.d.*) with *S. aureus* (SA), and *Camp* mRNA expression (ratio to housekeeping gene *Tbp*) in skin or spleen tissues were measured by RTqPCR analyses

(n=3~5/group). (**C**). Measurement of bacterial CFU from the infection edge area of the skin from infected *Camp*$^{f/f}$ or *Camp*$^{f/f}$*Pdgfra-cre* mice (n=6/group). (**D**). 3 weeks, 2 months, 1 year or 2 years wildtype mice were infected i.d. with *S. aureus*, and bacteria CFU were measured from the infection edge area (n=4~5/group). (**E**). Cathelicidin (red) and COLIV (green) IHC staining in control or *S. aureus* infected skin (representative of n=3/group). Nuclei were stained by DAPI (blue). Scale bar, 100 μm. (**F**). RTqPCR of *Camp* or *Spp1* expression in the infected skin or controls skin (ratio to *Tbp*) (n=3~5/group). (**G**). Flow cytometry plots for gating strategies for dermal PDGFRA^{+}THY1^{hi} adipocyte progenitors (representative of n=3/group). (**H**). Flow cytometry quantification of the geometric MFI (gMFI) of Sca1 expression in THY1^{lo} or THY1^{hi} CD31^{-}CD45^{-}PDGFRA^{+} dFB in control or *S. aureus* -infected skin (n=3/group). (**I**). Flow cytometry plots of THY1 and PDGFRA in CD31^{-}CD45^{-}PDGFRA^{+} FB in skin dermis or eWAT. (**J**). Overlaid histogram of THY1 expression in CD31^{-}CD45-PDGFRA^{+} FB in skin dermis or eWAT (representative of n=3/group). (**K**). Stacked bar graphs showing age-dependent changes of the percentage of THY1^{lo}, THY1^{med} and THY1^{hi} in CD31^{-}CD45-PDGFRA^{+} FB in skin dermis or eWAT (average of n=3/group). (**L**). Age-dependent changes of the percentage of THY1$^{lo\text{-}med}$PDGFRA^{+} fibroblasts, THY1^{hi}PDGFRA^{+} fibroblasts, CD11B^{+}F4/80^{+} macrophages, CD11B^{+}Ly6G+ neutrophils, CD11C^{+}F4/80^{-} dendritic cells, CD45^{+}TCRγδ+ T cells and CD45^{+}TCRαβ+ T cells in total dermal cell population as indicated (average of n=3/group). All error bars indicate mean ± s.e.m. * P<0.05, ** P<0.01, *** P<0.001 (One way Anova). Please see also Figure S1.

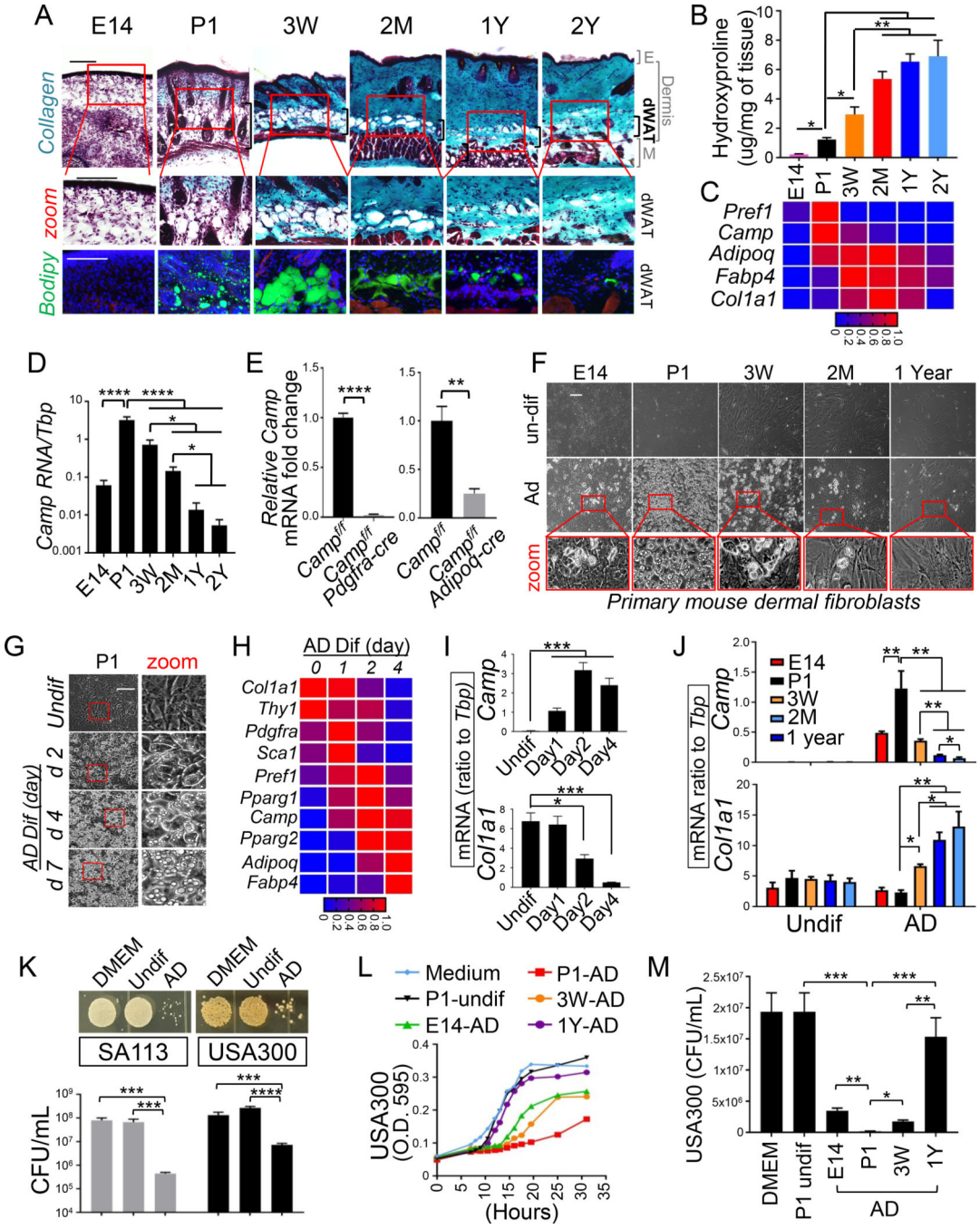

Figure 2. Loss dermal immature fat and adipogenic-antimicrobial function of primary dFB during development and aging of mouse skin.

(**A**). Gomori Trichrome staining (upper panel) or lipid Bodipy (green) and phalloidin (red) staining (lower panel) of skin sections from mice at indicated age (representative of n=3~6/group). (**B**). Hydroxyproline content (ug per mg of tissue) in mouse dorsal skin at indicated age (representative of n=3/group). (**C**). Heatmap showing the mRNA expression kinetics of listed pAd or Ad genes in mouse skin at indicated age (average of n=3/group). (**D**). *Camp* mRNA expression kinetics in mouse skin at indicated age (n=3/group). (**E**). Relative *Camp*

mRNA expression in skin isolated from neonatal *Camp*$^{f/f}$ or *Camp*$^{f/f}$*Pdgfra-cre* or *Camp*$^{f/f}$;*Adipoq-cre* neonatal littermates (n=3/group). **(F)**. Phase contrast images showing age-dependent alterations in the adipogenic potential of primary dFB (representative of n=3/group). (**G**). Phase contrast images showing time course adipocyte differentiation from neonatal P1 dFB (representative of n=3/group). (**H**). Heatmap showing kinetics of pAd/Ad gene mRNA expression during adipocyte differentiation of P1 dFB (average of n=3/group). (**I**). Bar graphs of mRNA expression kinetics of *Camp or Col1a1* gene during adipocyte differentiation of P1 dFB (average of n=3/group). (**J**). *Camp or Col1a1* mRNA expression in undifferentiated dFBs or differentiated adipocytes (n=3~5/group). (**K**). SA113 or USA300 growth image on agar plate or CFU count of bacterial growth in conditioned medium (CM) P1 AD or undifferentiated cells or DMEM (n=3/group). (**L-M**). Growth curve (**L**) or CFU count (**M**) of *S. aureus* in CM from undifferentiated dFB or differentiated adipocytes at indicated age (n=3~5/group). All error bars indicate mean ± s.e.m. * P<0.05, ** P<0.01, *** P<0.001 (one way Anova). All scale bars are 100 μm. Please see also Figure S2.

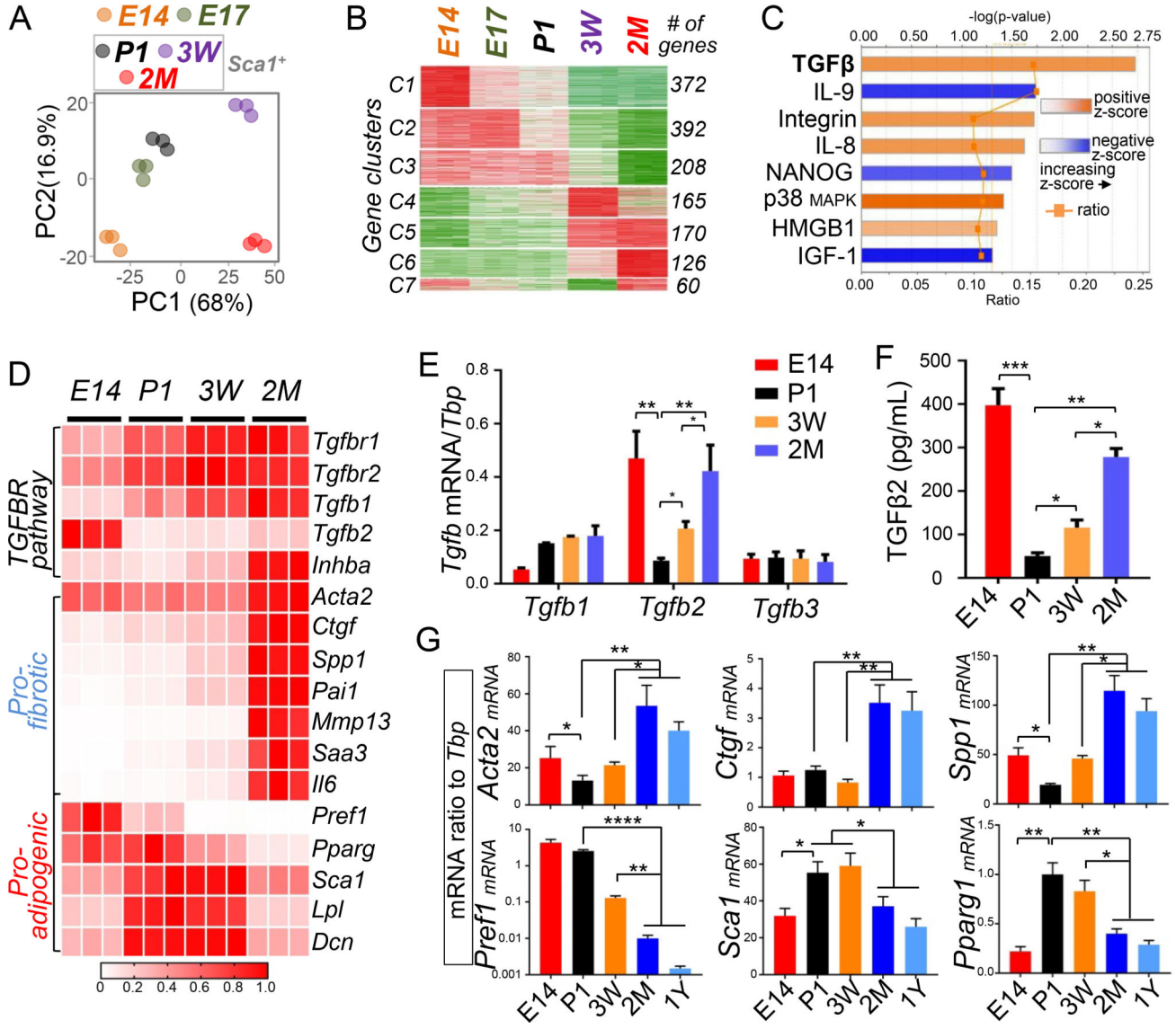

Figure 3. Activation of the TGFβ pathway is associated with the loss of antimicrobial function of dFB.

(**A**). Principle component analysis plot for RNA-seq showing differential clustering of E14, E17 or Sca1^{+} sorted P1, 3 week and 2 month dFB. Dots with the same color represent biological replicates in indicated age group (n=3/age group). (**B**). Time course analyses by maSigPro identified 7 gene clusters with distinct expression dynamics in dFB from E14 ~ 2 month as indicated. # of genes in each cluster is indicated on the right. (**C**). Ingenuity Pathway Analysis (IPA) identified several signaling pathways that were activated (orange) or inhibited (blue) in 2 month Sca1^{+} dFB compared to P1 Sca1^{+} dFB. Respective –log(p-value), z-score and ratio is shown for each pathway. The calculated z-score indicates a pathway with genes exhibiting overall increased mRNA (orange bars) or decreased mRNA expression (blue bars). The ratio (orange dots connected by a line) indicates the ratio of genes from the dataset that map to the pathway divided by the total number of genes that map to the same pathway, e.g. >15% for TGFβ signaling. (**D**). Heatmap showing relative

mRNA expression (based on RNA-seq derived RPKM values) of a panel of TGFBR pathway gene, pro-fibrotic genes or pro-adipogenic genes in primary dFB (average of n=3/group). (**E**). RTqPCR analyses showing mRNA expression of TGFβ family genes (ratio to *Tbp*) in dFB at indicated ages (n=3/group). (**F**). TGFβ2 protein secretion (pg/mL) in the conditioned medium of dFB was quantified by ELISA (n=3/group). (**G**). RTqPCR analyses validating age-dependent changes of mRNA expression of pro-adipogenic genes (*Pref1, Sca1* and *Pparg1*) or pro-fibrotic genes (*Acta2, Ctgf and Spp1)* (n=3/group). All error bars indicate mean ± s.e.m. * P<0.05, ** P<0.01, *** P<0.001 (one way Anova). Please see also Figure S3.

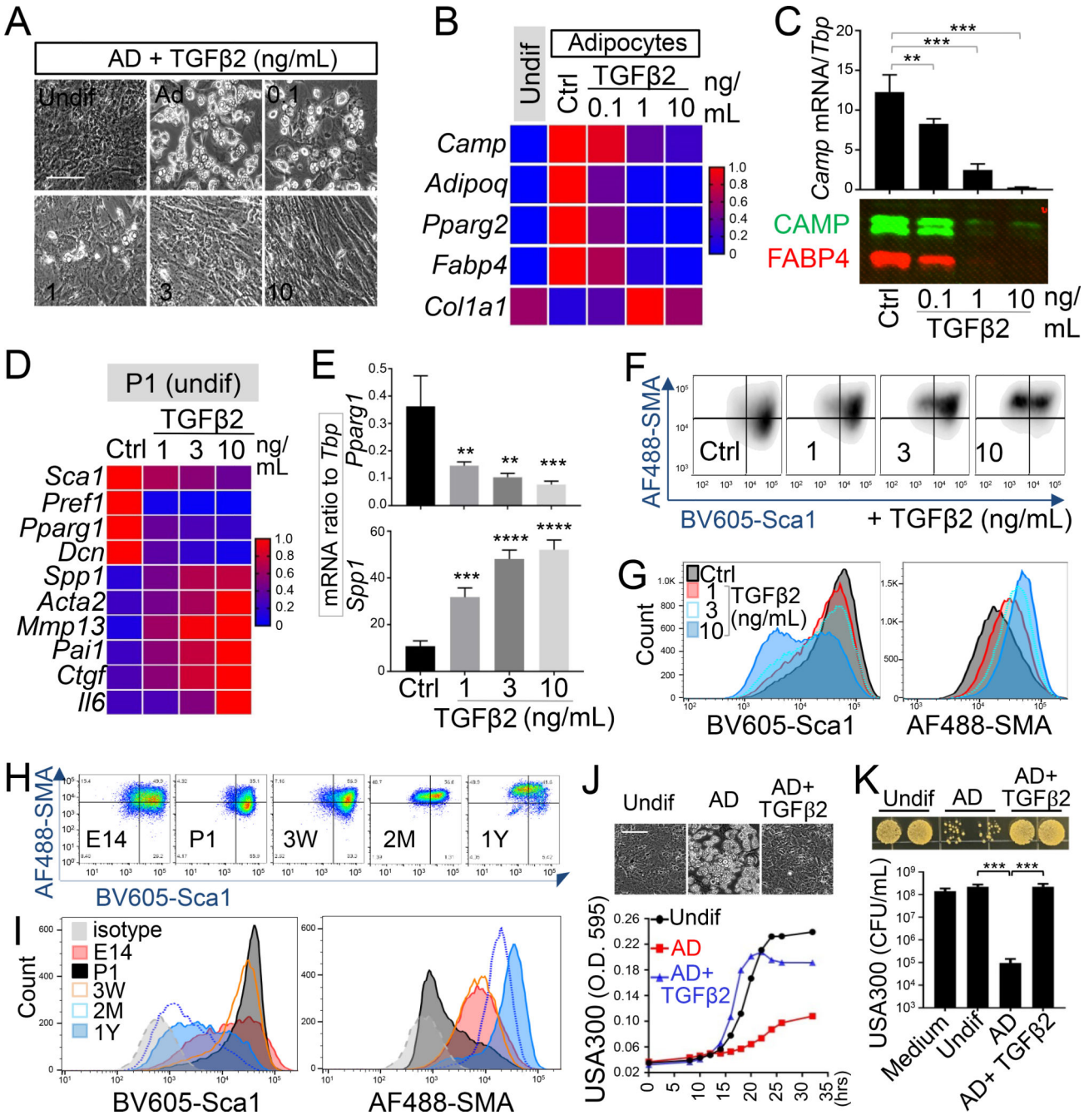

Figure 4. TGFβ2 drives a loss of adipogenic-antimicrobial function of neonatal dFB.

(A-C). Neonatal dFB were treated with increasing doses of TGFβ2 and differentiated in adipocytes. (**A**). Phase contrast images showing adipocyte formation at day 4 (representative of n=3/group). Scale bar, 100 μm. (**B**). Heatmap showing the effect of TGFβ2 in suppressing the mRNA expression of adipocyte genes (average of n=3/group). (**C**). *Camp* mRNA expression was measured by RTqPCR (top bar graphs) and CAMP and FABP4 protein secretion (lower western blotsl) (representative of n=3/group). (**D-G**). Neonatal P1 dFB were treated with increasing doses of TGFβ2 for 2 days under undifferentiated conditioned. Heatmap (**D**) or bar graphs (**E**) showing relative expression of pro-adipogenic or pro-fibrotic

genes as indicated (n=3/group). Flow cytometry plots (**F**) or overlaid histograms (**G**) of Sca1 and SMA (representative of n=3/group). **(H**). Flow cytometry plots of Sca1 and SMA in cultured PDGFRA^{+}THY1^{+} dFB with indicated age. (**I**). Overlaid histogram of Sca1 or SMA protein expression shown in H (representative of n=3/group). (**J**). Growth curve of USA300 in conditioned medium from undifferentiated dFB or differentiated adipocytes (n=3~5/group). Inserted phase contrast images show the effect of TGFβ2 in suppressing adipocyte formation. Scale bar, 100 μm. (**K**). Bacterial growth image on agar plate or CFU count of USA300 growth at 20 hours in conditioned medium from adipocyte treated with or w/o TGFβ2 as indicated (n=3~5/group). All error bars indicate mean ± s.e.m. * P<0.05, ** P<0.01, *** P<0.001 (one way Anova). Please see also Figure S4.

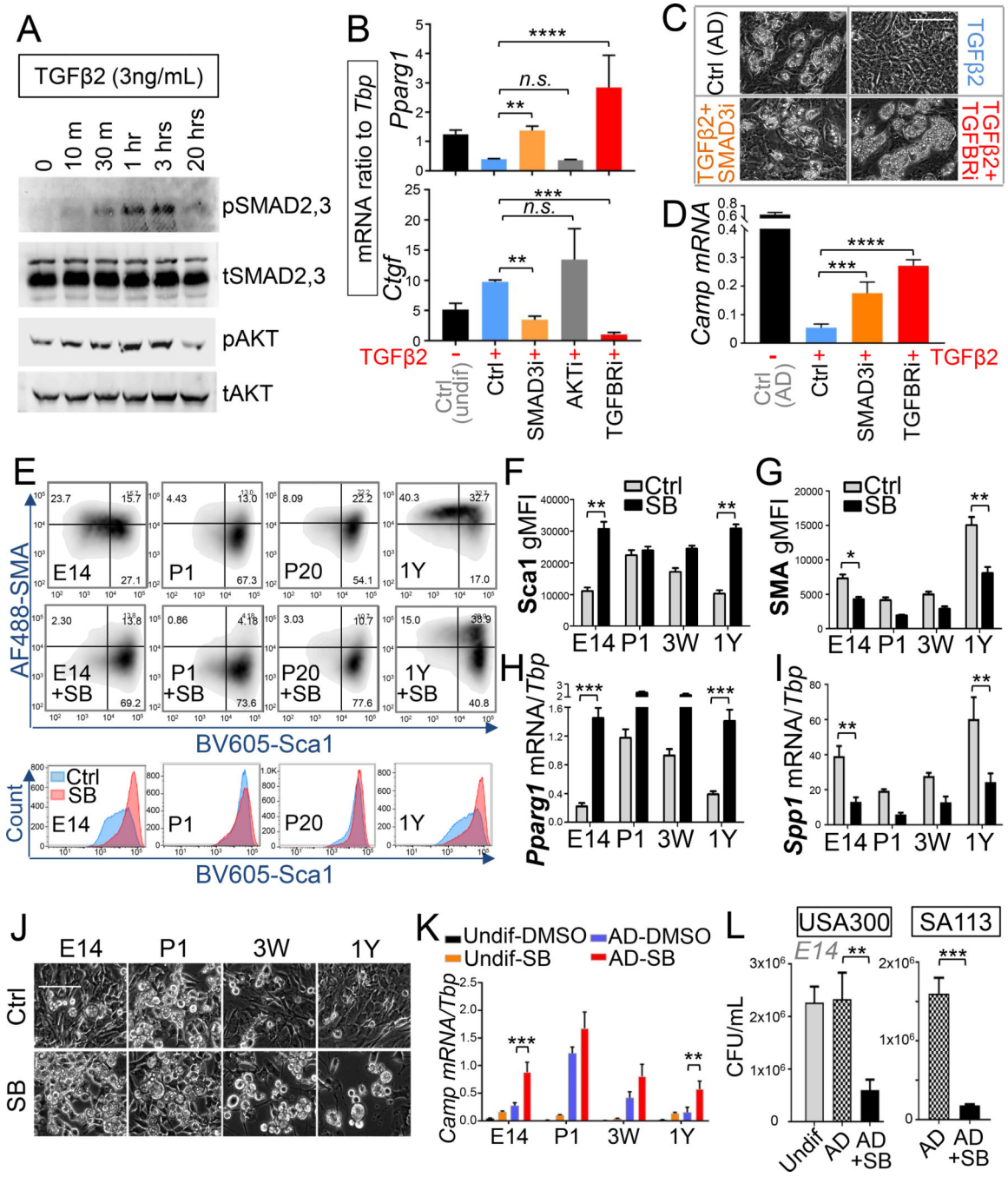

Figure 5. TGFβ mediates its pro-fibrotic and anti-adipogenic function by activating the TGFBR-SMAD2,3 pathway in dFB.

(**A**). Westernblot analyses of phosphor or total SMAD2,3 or AKT in P1 dFB treated with 3 ng/mL TGFβ2 for indicated time. (**B**). RTqPCR analyses of *Pparg1* or *Ctgf* mRNA expression in neonatal dFB pre-treated with specific inhibitors for SMAD3 (SIS3, 2 μM), PI3K-AKT (0.5 μM Wortmannin), or TGFBR (SB431542, SB, 5 μM) then TGFβ2 for 24 hours (n=3/group). (**C-D**). TGFβ2-mediated loss of adipogenic function of neonatal dFB can be rescued by SMAD3 or TGFBR inhibitor as shown by phase contrast images (**C**) or

RTqPCR analysis of *Camp* mRNA expression (**D**) (n=3/group). Scale bar, 100 μm. (**E**). Flow cytometry plots of Sca1 and SMA (upper two panels) or overlaid histogram of Sca1 (lower panel) in PDGFRA^{+}THY1^{+} dFB treated with TGFBR inhibitor SB431542 (representative of n=3/group). (**F-G**). Quantification of the geometric MFI of Sca1 or SMA protein expression shown in E (n=3/group). (**H-I**). *Pparg1* or *Spp1* mRNA expression in dFB treated SB or DMSO control for 2 days (n=3/group). (**J**). Phase contrast images of dFB differentiated to adipocyte in the presence of SB or DMSO control (representative of n=3/group). Scale bar, 100 μm. (**K**). *Camp* mRNA expression in undifferentiated or adipocyte-differentiated dFB treated with SB or DMSO control (n=3/group). (**L**). Inhibition of TGFBR by SB restored the antimicrobial activity of E14 embryonic dFB as shown by CFU counts of USA300 or SA113 growth at 20 hours (n=3~5/group). All error bars indicate mean ± s.e.m. * P<0.05, ** P<0.01, *** P<0.001 (one way Anova). Please see also Figure S5.

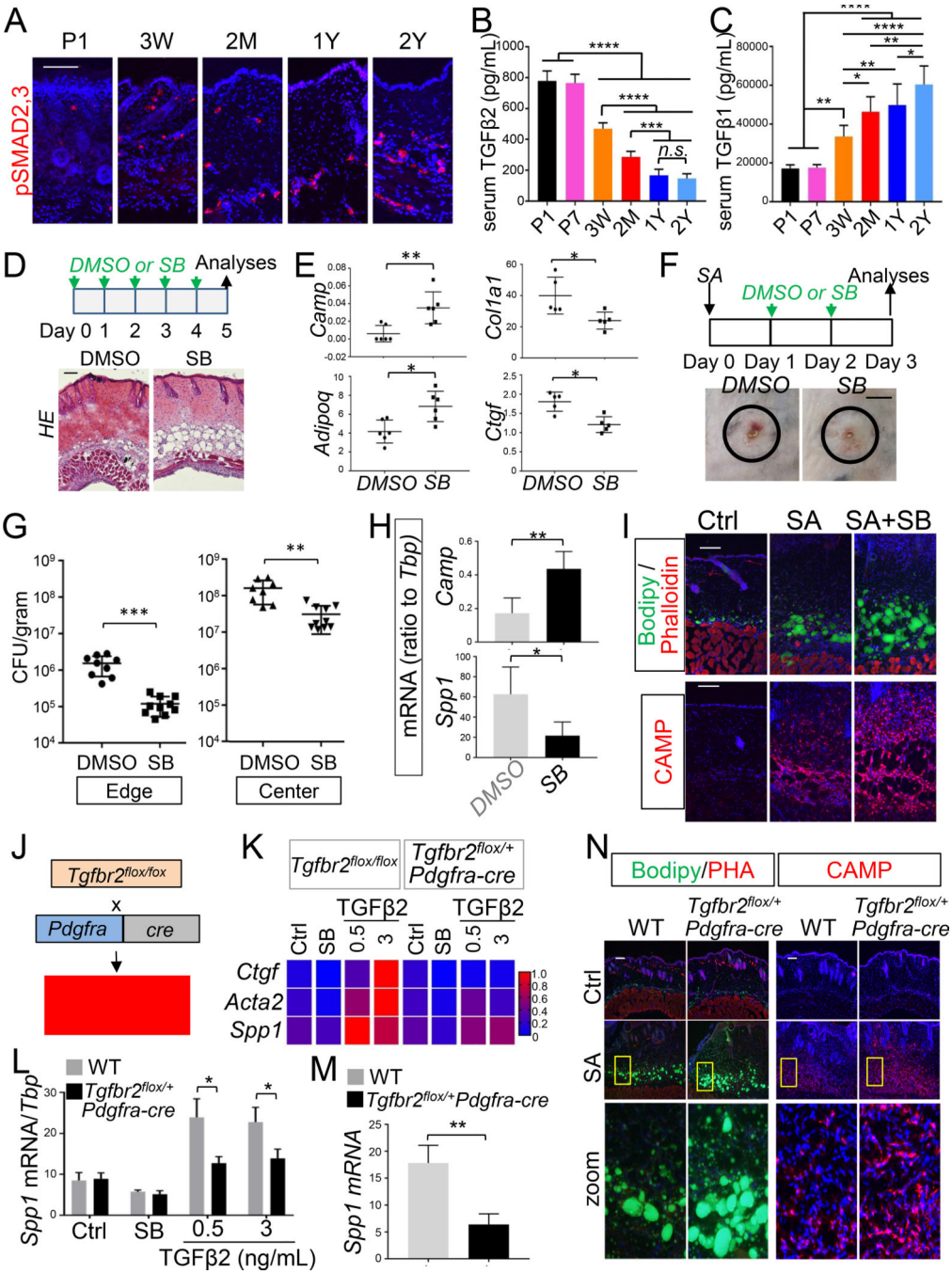

Figure 6. Inhibition of TGFBR function boosts dFB adipogenic potential and enhances resistance to skin infection.

(**A**). pSMAD2,3 immunostaining of skin sections from mice at indicated age (representative of n=3/group). (**B-C**). Measurement of serum concentrations of TGFβ2 (**B**) or TGFβ1 (**C**) in mice at indicated age (n=3~6/age group). (**D-E**). C57BL6 wildtype mice (2 mon, male) were treated i.d. with DMSO (control) or SB daily for 5 days and skin samples were collected for HE (**D**) or RTqPCR (**E**) analyses as indicated (representative of n=5~6/group). (**F**). Representative skin lesion pictures of 1 year old C57BL6 mice infected with *S. aureus* then

treated *i.d.* with DMSO or SB (n=5/group). (**G**). Bacterial CFU was measured from the infection edge or center area at day 3 (n=5 mice/group). (**H**). *Camp* and *Spp1* mRNA expression in *S. aureus* infected skin (n=3~5 mice/group). (**I**). Representative Bodipy staining or cathelicidin (CAMP) staining in infected skin (n=3~5 mice/group). Nuclei were stained by DAPI (blue). (**J**). Conditional heterozygous *Tgfbr2* deletion of *Tgfbr2* in *Pdgfra*$^{+}$ fibroblasts, *Tgfbr2*$^{flox/+}$*Pdgfra-cre*, was achieved by breeding *Tgfbr2*$^{flox/flox}$ mice with *Pdgfra-cre* mice. (**K-L**). Primary mouse dFB (WT or *Tgfbr2* $^{flox/+}$*Pdgfra-cre*) were treated with increasing dose of TGFβ2, and gene induction of *Ctgf*, *Acta2* and *Spp1* was shown in heatmap (**K**) or bar graph for *Spp1* (**L**) (n=3/group). (**M-N**). WT or *Tgfbr2* $^{flox/+}$*Pdgfra-cre* mice were infected *i.d.* with *S. aureus*. (**M**). mRNA expression of profibrotic gene *Spp1* in infected skin (ratio to *Tbp*) (n=3~5 mice/group). (**N**). Skin biopsies were subjected to Bodipy staining or cathelicidin staining as indicated (representative of n=3~5/group). Nuclei were stained by DAPI (blue). All error bars indicate mean ± s.e.m. * P<0.05, ** P<0.01, *** P<0.001 (one way Anova). All scale bars are 100 μm. Please see also Figure S1.

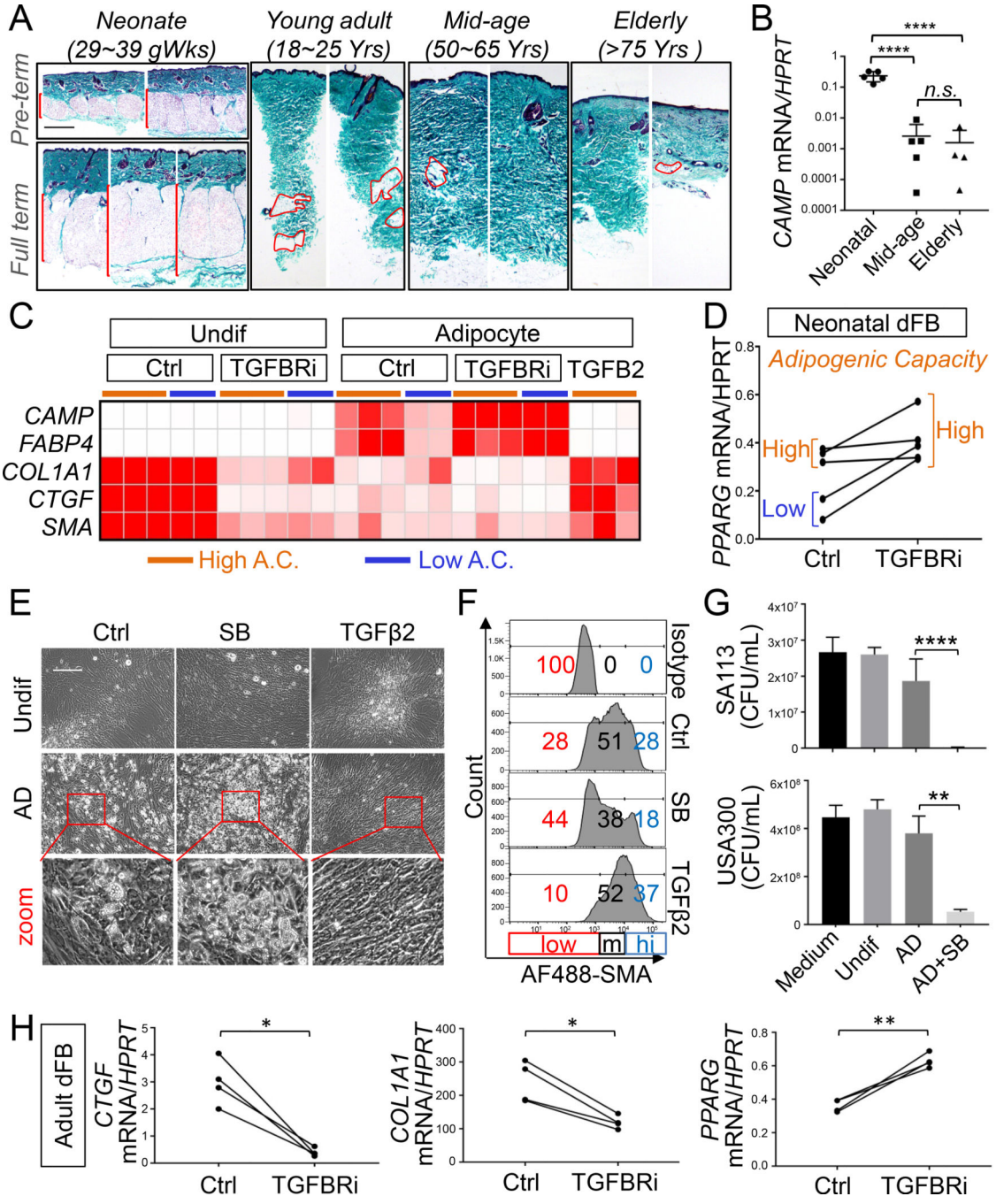

Figure 7. TGFβ promotes loss of adipogenic and antimicrobial defense function of primary human dermal fibroblasts.

(**A**). Representative collagen trichrome staining images of human back skin sections from neonates (pre-term: gestation week, GW 29~32 or full term GW 38~40), young adult (18~25 years), mid-age adult (50~65 years) and elderly (>75 years). All subjects are white Caucasians (n=3~6/age group). DWAT is highlighted by red bracelet or dotted lines are shown in the lower left panels. Scale bar, 100 μm. (**B**). RTqPCR analyses of *CAMP* mRNA expression (ratio to housekeeping *HPRT*) in human neonatal, mid-age or elderly skin as

indicated (n=4~5/group). (**C**). Human dFB isolated from 5 neonatal donors were differentiated to adipocytes with or without TGFBR inhibitor or TGFβ2. Heatmap showing the mRNA expression of indicated genes in undifferentiated or differentiated cells with high (orange line, n=3) or low (blue line, n=2) basal adipogenic capacity (A.C.). (**D**). RTqPCR analysis of *PPARG* mRNA expression in neonatal dFB (with high or low basal A.C.) treated with or without TGFBR inhibitor for 48 hours (n=5/group). (**E-G**). Primary human neonatal dFB (with low basal A.C.) were differentiated to adipocytes with or without TGFBR inhibitor (SB) or recombinant TGFβ2. (**E**). Phase contrast images (representative of n=3/group). Scale bar, 200 μm. (**F**). Flow cytometry histogram of SMA expression in undifferentiated dFB treated with SB or TGFβ2 (representative of n=3/group). (**G**). CFU count of *S. aureus* USA300 growth at 20 hours in conditioned medium from undifferentiated cells or adipocyte differentiated cells as indicated (n=3~5/group). (**H**). Primary adult human dFB were isolated from 4 mid-age donors' back skin. RTqPCR analyses of *CTGF*, *COL1A1* and *PPARG1* in adult dFB treated with vehicle control or TGFBR inhibitor (n=3~4/group). All error bars indicate mean ± s.e.m. * P<0.05, ** P<0.01, *** P<0.001 (one way Anova). Please see also Figure S6 and S7.

KEY RESOURCES TABLE

REAGENT or RESOURCE	SOURCE	IDENTIFIER
Antibodies		
Rabbit anti-CRAMP	University of California San Diego	Dr. Richard Gallo
Rabbit anti-LL37	University of California San Diego	Dr. Richard Gallo
goat anti-COLIV	Abcam	ab769
Mouse anti-FABP4	Abcam	ab188387
Rabbit anti-Phospho-SMAD2, 3	Cell Signaling	8828S
Rabbit anti-SMAD2,3	Abcam	ab202445
rabbit anti-phospho-AKT antibody	Cell Signaling	4060S
mouse anti-AKT	Cell Signaling	4691S
anti-mouse CD16/32	eBioscience	14016185
PECy7 anti-CD45	BioLegend	147704
PerCP-Cy5.5 anti-CD31	BioLegend	102522
PE anti-THY1	BioLegend	105308
APC anti-PDGFRA	eBioscience	17140181
BV605 anti-Sca1	BioLegend	108133
AF488 anti-SMA	eBioscience	53976082
APC anti-CD4	Biolegend	100516
BV510 anti-CD8a	Biolegend	100752
APC-Cy7 anti-TCRβ	Biolegend	109220
PE anti-TCRδγ	eBioscience	12-5711-82
PerCP-Cy5.5 anti-CD45.2	Biolegend	109828
PECy7 anti-CD11B	Biolegend	101216
FITC anti-Ly6G	eBioscience	11593182
PE anti-F4/80	eBioscience	56532182
APC anti-CD11C	Biolegend	117310
AF700 anti-MHCII	eBioscience	56532182
zombie violet viability dye	Biolegend	423114
Bodipy	ThermoFisher Scientific	D3922
Bacterial and Virus Strains		
S. aureus USA300	University of California San Diego	Dr. Victor Nizet
S. aureus SA113	University of California San Diego	Dr. Victor Nizet
Biological Samples		
Mouse skin, spleen, blood samples	University of California San Diego, Animal Facility	N/A
Neonatal human skin samples	International Institute for Advancement of Medicine (IIAM)	N/A
Adult human skin samples	University of California San Diego, Dermatology clinics	N/A
Chemicals, Peptides, and Recombinant Proteins		

REAGENT or RESOURCE	SOURCE	IDENTIFIER
SB431542	Selleckchem	S1067
SIS3	Selleckchem	S7959
Wortmannin	EMD Millipore	9951
3-Isobutyl-1-methylxanthine (IBMX)	SIGMA-ALDRICH	I5879
Indomethacin	SIGMA-ALDRICH	I8280
Dexamethasone	SIGMA-ALDRICH	D4902
Insulin	SIGMA-ALDRICH	91077C
DMEM, high glucose	Thermo Fisher Scientific (Life Technologies)	11965118
Antibiotic-Antimycotic	Thermo Fisher Scientific (Life Technologies)	15240062
Glutamax	Thermo Fisher Scientific (Life Technologies)	35050-061
Recombinant mouse TGFβ1	R&D Systems	7666-MB-005
Recombinant mouse TGFβ2	R&D Systems	7346-B2-005
PureLink RNA Mini Kit	Thermo Fisher Scientific (Life Technologies)	12183025
Collagenase D from Clostridium histolyticum	Roche	11088882001
Deoxyribonuclease I from bovine pancreas,Type IV, lyophilized powder	SIGMA-ALDRICH	D5025-150KU
RNase-free DNase Set	Qiagen	79254
iScript cDNA synthesis kit	Bio-Rad	1725038
2x SYBR Green qPCR Master Mix	Bimake	B21202
Super Script II Reverse Transcriptase	Invitrogen	18064014
KAPA HiFi Hotstart ReadyMix	Kapa Biosystems	KK2601
AMPure XP beads	Beckman Coulter	A63881
Critical Commercial Assays		
Gomori Trichrome green collagen staining kit	ThermoFisher Scientific	87021
Hydroxyproline assay kit	BioVision	K555-100
Mouse TGF-beta 1 ELISA	R&D Systems	DY7346-05
Mouse TGF-beta 2 ELISA	R&D Systems	DY7346-05
Intracellular Fixation & Permeabilization Buffer Set	eBioscience	88-8824-00
Nextera DNA Sample Preparation kit	Illumina	FC-121-1030
NextSeq 500 High Output Kit v2 – 75 cycles	Illumina	FC-404-2005
Deposited Data		
RNA-seq data of cultured E14 ~ 2 month dermal fibroblasts	NCBI Gene Expression Omnibus (GEO)	GEO accession #: GSE121460
Experimental Models: Cell Lines		
Primary mouse or human dermal fibroblasts	This study	Isolated from mouse or human skin dermis
Experimental Models: Organisms/Strains		
Camp$^{flox/flox}$ mice	This study	Dr. Richard Gallo

REAGENT or RESOURCE	SOURCE	IDENTIFIER
Pdgfra-cre mice	Jackson laboratory	013148
Adipoq-cre mice	Jackson laboratory	028020
Tgfbr2$^{flox/flox}$	Jackson laboratory	012603
Oligonucleotides		
Mouse primers for RTqPCR	Integrated DNA Technologies (IDT)	See Table S1 for primer sequences
Human primers for RTqPCR	Integrated DNA Technologies (IDT)	See Table S2 for primer sequences
Software and Algorithms		
GraphPad Prism	GraphPad Software, Inc.	
FlowJo V10	FlowJo LLC	
Ingenuity pathway analysis	Qiagen	
Bowtie	Langmead et al. 2009	http://bowtie-bio.sourceforge.net/manual.shtml
RSEM	Li and Dewey, 2011	https://github.com/deweylab/RSEM
Next maSigPro	Nueda et al. 2014	https://www.bioconductor.org/packages/release/bioc/html/maSigPro.html